Hindawi
Advances in Materials Science and Engineering
Volume 2022, Article ID 6858283, 21 pages
https://doi.org/10.1155/2022/6858283

Research Article

Effect of Joint Flexibility on Seismic Performance of a Reinforced Concrete Ductile Moment-Resisting Frame

Dagvabazar Gombosuren [1] and Takeshi Maki [2]

[1] *Department of Civil Engineering, School of Civil Engineering and Architecture, Mongolian University of Science and Technology, Ulaanbaatar, Mongolia*
[2] *Department of Civil and Environmental Engineering, Saitama University, Saitama, Japan*

Correspondence should be addressed to Dagvabazar Gombosuren; gombosuren.d@must.edu.mn

Received 23 August 2022; Revised 28 November 2022; Accepted 16 December 2022; Published 26 December 2022

Academic Editor: Dora Foti

Currently, the seismic collapse risk of modern code-conforming reinforced concrete (RC) frame structures is often evaluated without considering the behavior of the beam-column (BC) joints since joints designed to meet modern concrete design codes are assumed to be sufficiently rigid. BC joints in RC ductile moment frames may undergo a significant amount of inclined cracking during strong earthquakes. Consequently, the stiffness, strength, and dynamic characteristics of the RC moment frames may vary. Hence, the rigid joint assumption may be unsuitable for assessing the seismic performances of RC ductile moment frames because the local strength and ductility demands of the constituent members can be misinterpreted by structural analyses based on the assumption of a rigid joint. In this study, nonlinear static and dynamic analyses are conducted to quantify the seismic response variations of low- to midrise RC-frame structures under different joint modeling assumptions. In total, six 2D continuum finite element models of four- and eight-story frames with rigid and flexible joints were constructed by simulating the actual structures as realistically as possible. The results indicate that the interior joints in the considered frames suffer light-to-moderate damage, and the effect of joint cracking is found to be significant in a four-story structure whose column-to-beam flexural strength ratio and column-to-beam area ratio are below 1.5. Such joint behavior demonstrates that current code provisions cannot ensure joint behavior compatible with the rigid joint assumption that is used in the practical structural analysis of RC-frame buildings.

1. Introduction

Forensic investigations of earthquake-induced failures [1, 2] revealed that a failure of poorly designed beam-column (BC) joints is one of the most undesirable failure modes for reinforced concrete (RC) moment-resisting frame (MRF) buildings under seismic action. Hence, the joints connecting the columns and beams should not be weak links during a seismic attack because their failure can potentially lead to the loss of structural integrity and the eventual collapse of the structures [3, 4]. Therefore, to prevent joint brittle failure, modern concrete design codes [5–8] include special proportioning and detailing requirements for BC joints in RC MRF buildings; these are based on extensive laboratory test results.

The effect of the cyclic behavior of BC joints on the seismic performances of MRF structures has received less attention as compared with that of beams and columns. This relates to the fact that the majority of existing experimental and analytical studies over the past few decades [9–16] have focused exclusively on the shear behaviors of BC joint panels separated from adjacent beams and columns. Accordingly, the seismic design of BC joints was formulated primarily based on the joint shear stress with less emphasis placed on joint deformation; this force-based design approach was introduced in the 1990s. Since then, empirical joint strength equations have been adopted into the design codes [5–8]. It is now believed that joints designed to satisfy modern code requirements are unlikely to fail. Thus, in structural analyses of RC MRF building systems subjected to seismic excitations, BC joints are typically modeled with rigid joint panels (i.e., rigid member-end offsets in a centerline model), irrespective of the joint details.

However, experimental and numerical investigations [17–20] have shown that BC joints in RC ductile MRF structures designed according to current codes may undergo a significant amount of diagonal cracking during a strong earthquake event. Moreover, other studies [21–23] have reported that inclined cracking in interior joints conforming to the requirements of modern design codes was initiated at nominal shear stresses of approximately $0.4\sqrt{f'_c}$ to $0.6\sqrt{f'_c}$ (MPa), less than 40% of the nominal joint strength (1.25 to 1.5 $\sqrt{f'_c}$). Thus, it is now known that "joint shear stress" is a useful index for the induced force level but is not suitable for assessing joint deformation demand. In this context, a concept of the "joint shear deformation index (SDI) was introduced by the authors of reference [23] to consider the effect of joint deformation on the structural response of RC frames. Assuming that the joint deformation of the BC joint contributes to the total story drift, the SDI is defined as the ratio of the lateral drift ratio R_{sps} due to the joint shear deformation to the total lateral drift ratio R_s.

The authors compiled 58 available experimental results (including their eight specimens) reported in the previous investigations to find out the most important parameters affecting joint deformation. The experimental database encompassed a wide range of interior BC joints found rather common in low to midrise existing RC MRF structures. The collected experimental data can be found in Appendix C of the author's previous work [23]. Out of 58 specimens, 22 specimens with joint reinforcement ratios (ρ_j) of $\leq 0.7\%$ were reported to show joint failure before beam yielding (*J*-type failure), and 17 specimens with $0.5 \leq \rho_j \leq 1.6\%$ exhibited joint failure after beam yielding (BJ-type failure). 19 specimens having $0.5 \leq \rho_j \leq 1.3\%$ failed due to beam flexure (*B*-type failure). From the database, the SDI for each test specimen was evaluated to see how much joint deformation affects the joint failure modes. Figure 1 shows the correlation between the SDI and the combination of design parameters, and Figure 2 depicts the qualitative presentation of the three joint failure modes. It is assumed that the structural deformation is 3.5% for collapse prevention, which is slightly less than that defined in ASCE/SEI 41-13 standard [24] (referred to hereafter as ASCE 41). Here, the area of adjoining members (A_c/A_b) and column-to-beam flexural strength ratio ($\sum M_c/\sum M_b$) were considered as the parameters since the joint shear deformation exhibited a strong correlation with A_c/A_b and $\sum M_c/\sum M_b$.

In Figure 1, the contribution of the joint deformation to the total deformation of the BC joint connections tends to decrease as the value of the combined parameter increases. However, the range of the SDI values was 0.2 to 0.8 at a lateral drift ratio of 3.5% for BC joints falling into a red-dashed rectangular frame (Figure 1). This implies that the main source of the overall deformation of a BC joint sub-assemblage is joint deformation. Consequently, the global displacement ductility of the sub-assemblage is reduced (Figure 2). It should be noted that these joints satisfy the minimum requirements of modern concrete design codes. The behavior of such joints may considerably influence the

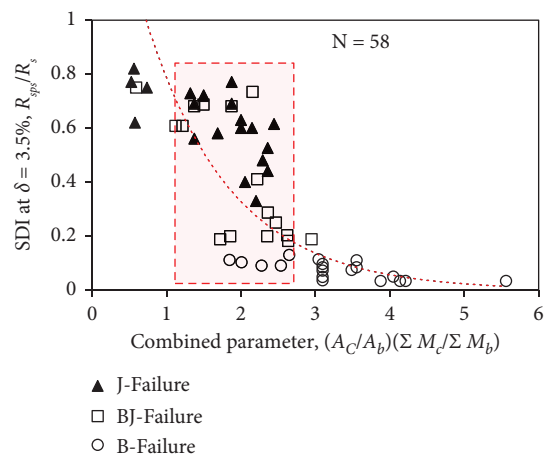

Figure 1: Correlation between the joint shear deformation index (SDI) and combined parameter.

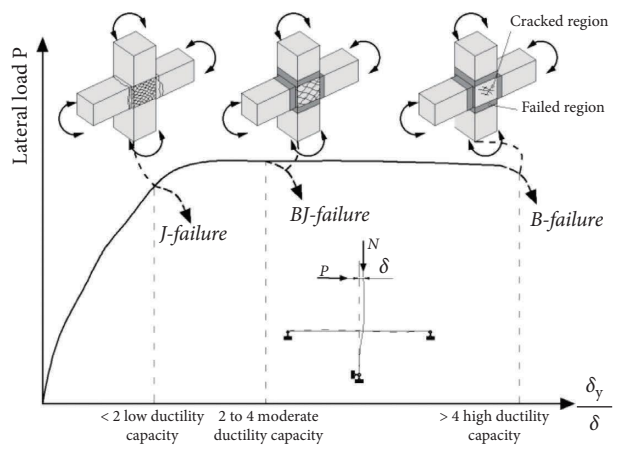

Figure 2: The three joint failure modes.

stiffness, strength, and dynamic characteristics of RC MRF structures during strong earthquakes. Thus, the rigid joint assumption may be unsuitable when evaluating the seismic performance of modern code-conforming RC ductile MRF structures because the local strength and ductility demands of the constituent members can be misinterpreted by structural analyses based on the assumption of a rigid joint.

A considerable number of studies [25–31] have investigated the effects of the behavior of nonconforming BC joints (i.e., joints that lack sufficient shear reinforcement and do not conform to the requirements of modern design codes) on the seismic behavior of gravity-load designed (GLD) RC frames. For instance, Bayhan et al. [31] analytically studied the effect of the behaviors of unreinforced BC joints on the responses of a seven-story GLD RC frame using a joint spring model. The backbone curve developed by Park and Mosalam [32] was used to define the moment-rotation relationship of the joint springs. The results of these studies showed that the lateral deflection of the frames significantly increased, whereas the curvature ductility demands on the beams and columns decreased when inelastic joint shear deformation was modeled.

Despite these significant achievements, few studies [18–20] have addressed the effects of the flexibility of modern code-conforming joints on the seismic responses of RC ductile MRF structures subjected to strong ground motions. Furthermore, most existing studies have utilized "multispring" models to simulate joint flexibility and "fiber section" or "plastic hinge" models to simulate the behavior of beams and columns for reducing computational effort in nonlinear analysis. However, the accuracy and reliability of these models highly depend on the calibration of empirical factors to incorporate the numerous parameters affecting joint seismic response. Moreover, such models do not account for the nonlinear interaction of structural components and their influence on the building system's performance. To produce accurate and reliable benchmark results, the structural model needs to accurately predict the structural response from low deformation levels (where cracking and tension-stiffening are important) to high deformation levels (where deterioration leading to collapse is important). Therefore, in this study, a two-dimensional (2D) continuum finite element (FE) investigation was conducted to accurately predict the seismic behavior of RC MRF structures under different joint modeling assumptions. To achieve this goal, nonlinear static and dynamic analyses were performed on four- and eight-regular RC MRF building systems without unreinforced masonry infill walls, representing low- to midrise structures. These buildings are designed and detailed according to the ACI 318-19 design code provisions for high seismic regions [5]. Six 2D FE models of four-andeight-story frames with rigid and flexible joints were constructed by simulating actual structures as realistically as possible. The main objective of this study was to evaluate the effects of joint flexibility on the expected performance of similar structures designed and constructed according to modern building code provisions. The performance estimates considered in this study include global responses and damage to structural members. We envision that the main findings will provide information to code committees that will allow them to calibrate building code provisions to produce desired levels of societal protection.

2. Code-Conforming RC Frame Structures

2.1. Selection of Buildings: Characteristics and Configuration. The buildings under investigation were four- and eight-story RC ductile MRF buildings that are believed to represent the seismic performance of a broad class of low- to mid-rise office building construction in the highly seismic regions, as shown in Figures 3 and 4. The buildings are regular in plan and elevation. The RC office building considered has four bays of 5.9 m in the longer direction and two bays of 6.5 m in the shorter direction (Figure 3). The story height for each level is 3.6 m. In practice, perimeter frames are considered a lateral force-resisting system, so the lateral load is allocated to them; meanwhile, interior frames are more flexible and mainly carry gravity loads. Compared with the perimeter frames with 4 bays, the two-bay perimeter frames have less lateral strength and stiffness, consequently making them more vulnerable to seismic attack. Hence, the two-bay, four-, and eight-story perimeter frames (Figures 4(a) and 4(b)) were selected. The four- and eight-story frames are hereafter referred to as "PF4" and "PF8." The seismic performance assessment is carried out for the RC building without unreinforced masonry infill walls, which is normally not considered in the analysis and design process.

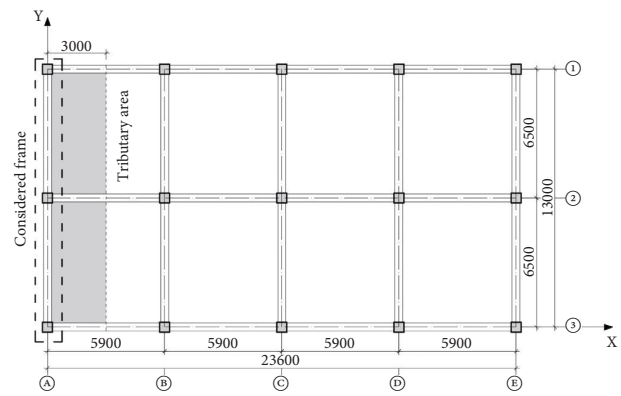

Figure 3: Plan view of the RC office building.

2.2. Seismic Design Procedure. Each RC MRF building was designed and detailed according to the ACI 318-19 design code provisions for high seismic regions. The codes of practice for earthquake-resistant structures (ASCE 7–10) [33] were used as a reference method of analysis, "the lateral force method analysis." The four-story building was designed to sustain a base shear of 20% of its total seismic weight, including the weight from gravity loads; meanwhile, the base shear for the eight-story building was 10% of its total seismic weight (a base shear coefficient of 0.1).

The floor slab's contribution to the flexural strength of the beams was neglected, though the self-weight of the slab was included in the seismic weight estimation. The slab thickness was assumed to be 150 mm. The cross-sectional dimensions and reinforcement arrangements of the beams and columns are illustrated in Figure 4. For Frame PF4, the exterior and interior columns had a 500 mm square cross-section (referred to as *C*1) over the height of the structure. On the other hand, a 600 mm square cross-section (referred to as *C*2) was used for the columns in Frame PF8. All the beams had a width of 400 mm and a depth of 600 mm. Frames PF4 and PF8 were regarded as reference frames. This is because static and dynamic analyses were performed not only on these two frames but also on their counterparts without joint shear reinforcement and the rigid joint assumption, respectively. The four- and eight-story frames with rigid joints were designated as PF4-R and PF8-R, respectively. PF4-noJH and PF8-noJH were assigned to the frames without joint shear reinforcement. The beams and columns of all frames were designed to provide sufficient shear reinforcement to prevent shear failure. The design of the BC joints in Frames PF4 and PF8 satisfies the minimum seismic requirements of ACI 318-19 and ACI 352-02 [34] in terms of the joint shear strength, column-to-beam flexural strength ratio, anchorage length, and joint transverse reinforcement. Moreover, the exterior and knee joints in PF4

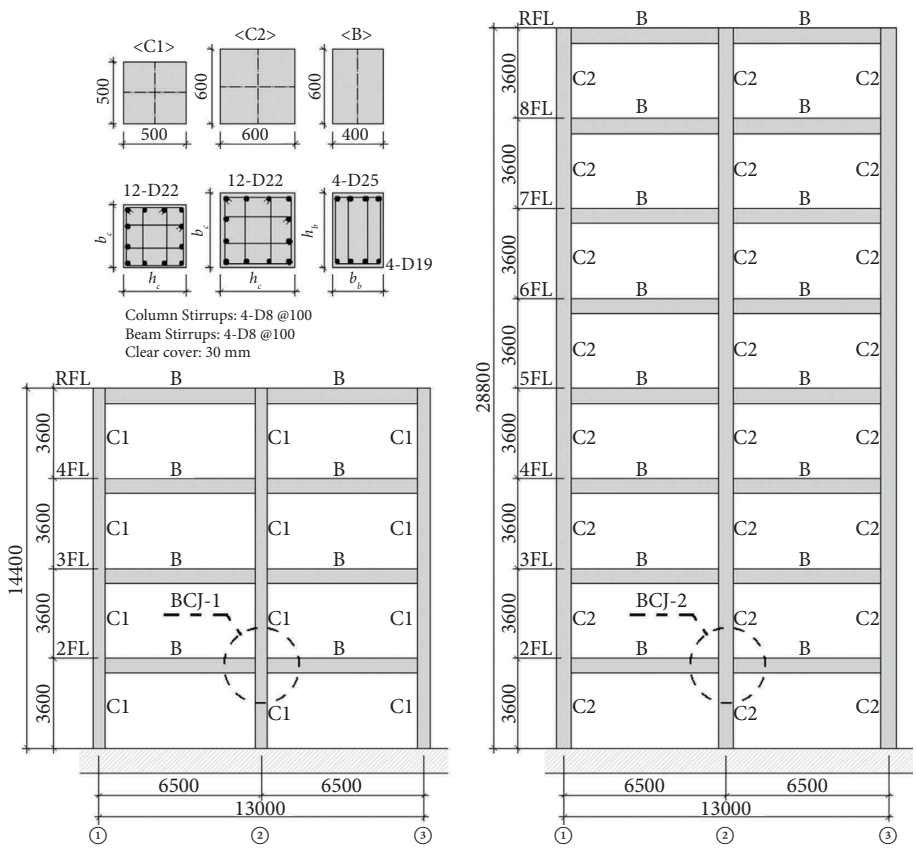

(a) (b)

Figure 4: Geometry and member dimensions (mm) for the four- and eight-story frames. (a) A four-story frame (PF4). (b) An eight-story frame (PF8).

and PF8 were designed to satisfy the relevant seismic requirements except for the end hooks and development length. In this study, the lateral deformation of the frames attributable to slippage of the bars is not considered. Hence, the effect of the lap-splice and anchorage details of the beam bars within the joint region on the response was neglected. In addition, the soil-structure interaction (SSI) was neglected because the main objective was to study the influence of joint flexibility in terms of the seismic response. Frames PF4, PF8, PF4-R, and PF8-R represent ductile-type RC buildings due to their conformity to modern seismic codes.

On the other hand, PF4-noJH and PF8-noJH were treated as nonductile-type RC buildings due to the absence of joint reinforcement. Table 1 presents the design details of the BC joints in Frames PF4 and PF8, and the reinforcing details of the joints are shown in Figure 5. The minimum amount of joint shear reinforcement in a single layer was computed according to the provisions of ACI 318-19 and ACI 352-02. Therefore, the total joint shear reinforcement ratios ($\rho_j = A_{sh,t}/b_c j$) were 0.6% and 0.66% for all joints in Frames PF4 and PF8, respectively. $A_{sh,t}$ represents the total cross-sectional area of the joint shear reinforcement (including crossties) within the distance j between the top and bottom beam longitudinal reinforcing bars; b_c represents the column width.

3. Finite Element Modeling

3.1. Description of FE Models. The FE analytical research program DIANA version 10.3 [35] was used to perform nonlinear static and dynamic analyses of the frames considered in this study. The accuracy and reliability of the nonlinear FE program have previously been verified against experimental results published by the authors [23] and other researchers [36–39]. The program was found to yield close predictions of the behavior of a wide range of RC structural forms under arbitrary static and dynamic loading conditions.

Six 2D continuum FE models of the four- and eight-story frames listed in Table 1 were constructed and analyzed. The main discrepancy between the analytical models of the four- and eight-story frames was that cracking could and could not form, respectively, within the BC joint regions. Moreover, the frames with flexible joints (i.e., PF4, PF4-noJH, PF8, and PF4-noJH) differed from one another in the case of only joint transverse reinforcement. In Frames PF4-R and PF8-R, the joints were modeled as elastic concrete elements set with double the elasticity modulus to simulate rigid joints. Consequently, cracking did not occur in the joint regions.

Figure 6 shows the FE model adopted for Frame PF4 as an example. The beams and columns were modeled using

Table 1: Design details of beam-column joints.

Frames	Frame PF4			Frame PF8			PF4-noJH	PF8-noJH	PF4-R	PF8-R
	Interior joint	Exterior joint	Knee joint	Interior joint	Exterior joint	Knee joint	All joints	All joints	All joints	All joints
Development length provided, h_c/d_b (mm)	500 (20)	445	445	600 (24)	545	545	All joint details are the same as those of frame PF4	All joint details are the same as those of frame PF8	All joint details are the same as those of frame PF4	All joint details are the same as those of frame PF8
Development length required—ACI 318	20	483	483	20	483	483				
Development length required—ACI 352	20.5	376	376	20.5	376	376				
Ratio of column capacity to beam moment capacity, M_R	1.5	−2.3 + 3.9	−1.2 + 2.0	2.1	−3.2 + 5.5	−1.6 + 2.8				
Ratio of joint shear capacity to shear demand	1.3	1.6	1.1	1.7	2.1	1.4				
Joint shear stress level, $v_j/\sqrt{f'_c}$	0.97	0.62	0.62	0.73	0.47	0.47				
Joint shear reinforcement ratio in a single layer, $A_{sh}/(s_h b''_c)$ (%)	0.81	0.81	0.81	0.76	0.76	0.76	W/o joint hoop	W/o joint hoop	W/rigid joint	W/rigid joint
Total joint shear reinforcement ratio, $\rho_j = A_{sh.t}/(b_c j)$ (%)	0.6	0.6	0.6	0.66	0.66	0.66				

The modulus of elasticity is $E_c = 25$ GPa and $E_s = 200$ GPa for concrete and steel, respectively. The uniaxial cylinder compressive strength of the concrete is $f'_c = 28.2$ MPa. The yield strength of the longitudinal reinforcing bars is $f_y = 431$ MPa, and the yield stress of the stirrups, ties, and joint hoops is $f_{yh} = 387$ MPa. Five layers of 4-D10 tie bars are placed in the joints of Frame PF4, whereas seven layers of 4-D10 tie bars are installed in those of Frame PF8. Thus, the area of a layer of 4-D10 is 285.32 mm^2, which is greater than the requirement of ACI 318-19: 216.2 mm^2 at 80 mm spacing and 192.5 mm^2 at 70 mm spacing. The flexural strength of the column is calculated at an axial load ratio of 0.1 $(N_u/f'_c A_g)$. Positive and negative signs indicate hogging and sagging moments of the beam end section, respectively.

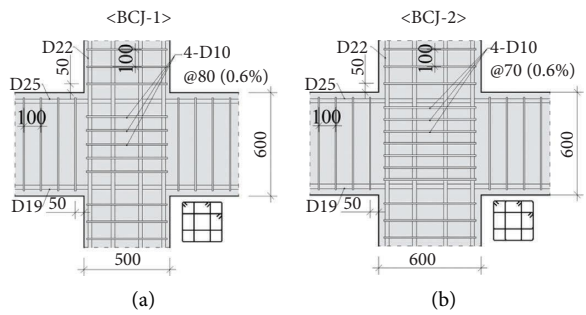

Figure 5: Details of joint shear reinforcements (units in mm). (a) Interior joints in frame PF4. (b) Interior joints in frame PF8.

eight-node quadrilateral plane stress elements, as depicted in Figure 6(b). The integration scheme for this plane stress element was selected as a 3×3 integration, which is suitable when the stiffness of the element becomes small under extensive cracking. The mesh size of the concrete element was $100 \times 100\ \mathrm{mm}^2$. The spacing of the stirrups in the vicinity of the intersection faces between the beams and columns was 100 mm, and it was increased to 200 mm in their mid-spans. It should be noted that the flanges of the beams were not incorporated in the FE model of each frame to simplify the analysis and reduce its cost. The horizontal and vertical movements at the bottom of the first-story columns were restrained to model the support conditions of the actual frame, as shown in Figure 6(b).

3.2. Modeling of Concrete. A total strain-based rotating smeared crack model was adopted for FE analysis. This model has been applied to the constitutive modeling of RC for a long time, and it has been demonstrated that the modeling approach is well-suited for RC structures [40]. In addition, the rotating crack model is suitable for localized cracking because it provides less shear stress locking than a fixed crack model. For this reason, the effect of steel reinforcement on RC structures can be investigated without the complications induced by concrete shear stress. This satisfies the secondary purpose of the present study, which is to determine the effect of the amount of joint shear reinforcement on the frame responses under strong ground motions. A constitutive model applied for concrete allows for tension, compression hardening, and softening, as well as the influence of lateral confinement.

3.2.1. Tensile Behavior. The nonlinear tension-softening model proposed by Hordijk [41] was employed since it resulted in more localized cracks and consequently avoided large areas of distributed cracking. The stress-strain relationship for concrete under tension is shown in Figure 7(a). Here, the tensile strength f_t, fracture energy G_f, and crack bandwidth h_{eq} are the governing parameters.

The compressive strength f_c' was used to determine the uniaxial tensile strength f_t of concrete in accordance with the CEB-FIB model code (2010) [42]:

$$f_t = 0.3\left(f_c'\right)^{2/3}. \tag{1}$$

The formula of the CEB-FIB model code was employed to determine the tensile fracture energy of the concrete (i.e., $G_f\,(N/\mathrm{mm}^2)$) as follows:

$$G_f = \frac{\left(73 f_c' 0.18\right)}{1000}, \tag{2}$$

where f_c' denotes the uniaxial cylinder compressive strength of the concrete (unit: in $\mathrm{N/mm}^2$).

The crack bandwidth h is an essential parameter in constitutive models. It describes the softening stress-strain relationship. In addition, it is crucial to reduce the mesh-size dependence. In this study, an automatic procedure was used to determine the crack bandwidth provided by the software. In this procedure, the area or volume of the FE was used to assign a value to the crack bandwidth. For higher-ordertwo-dimensional elements, the crack bandwidth was equal to $\sqrt{A}$, where A is the total area of the element.

3.2.2. Compressive Behavior. A parabolic stress-strain diagram with a softening branch for the compressive behavior of concrete was applied in this study (Figure 7(b)). The softening branch was determined according to the compressive fracture energy G_c to reduce the mesh-size dependence during compressive-strain localization. The compressive fracture energy of concrete $G_c\,(N/\mathrm{mm}^2)$ was determined using the formula proposed by Nakamura and Higai [43]:

$$G_c = 250 G_f. \tag{3}$$

The reduction in the concrete's compressive strength attributable to perpendicular tensile strain and cracks was considered using the model developed by Vecchio and Collins [44]. The effects of lateral confinement on the deformability of concrete were considered by modifying the compressive stress-strain curves, for which the parameters were determined by a failure function that defined the compressive stress as a function of the confining stresses in the lateral directions, as described by the model of Selby et al. [45].

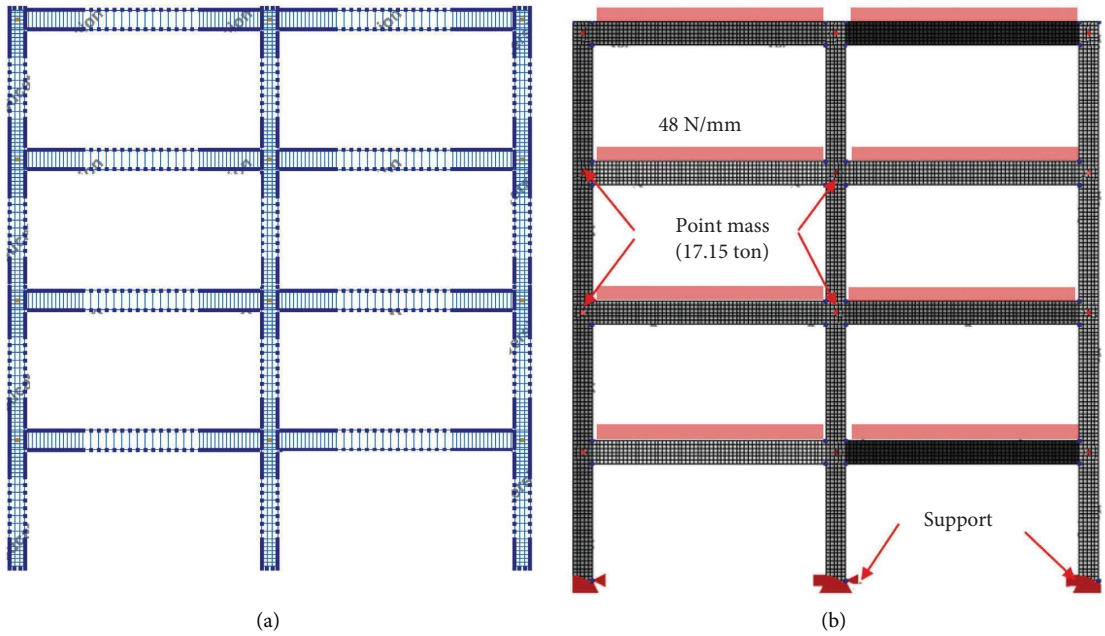

Figure 6: FE mesh of the frame structure. (a) Reinforcement elements. (b) Concrete elements.

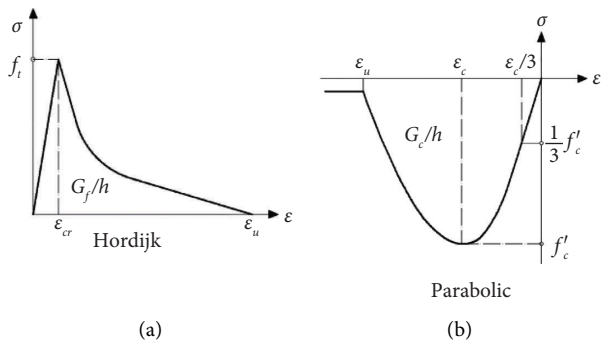

Figure 7: Constitutive model for concrete. (a) Predefined tensile stress-strain curve. (b) Predefined compressive stress-strain curve.

3.3. Modeling Reinforcement. The longitudinal and transverse reinforcing bars were modeled as embedded reinforcement elements with a perfect bond between the reinforcing bar and surrounding concrete (Figure 6(a)). This means that the bond-slip behavior of the reinforcing bars is not considered. For the exterior and knee joints, the reinforcing bars were simplified in the models by neglecting their end hooks, which are located in the actual BC joints. The reinforcement behavior was characterized by the von Mises yield criterion with isotropic strain hardening and the associated flow rule.

4. Nonlinear Static Analysis

Before the dynamic analysis, a nonlinear static analysis (NSA) or pushover analysis of the considered frames was undertaken to check the base shear strength and nonlinear responses of the structures, as well as to identify their possible failure mechanisms. Since the NSA was first introduced in the 1980s, many researchers [46–51] have developed NSA procedures to improve the accuracy and simplicity of the traditional NSA. The most important aspect of performing the NSA is to define a lateral load pattern that approximates the distribution of inertia forces. In this respect, ASCE 41 specifies an equivalent lateral force (ELF) modal distribution for regular low- to midrise RC-framed buildings. This ELF is approximately proportional to the shape of the fundamental mode in the direction under consideration. Entering such a schematized load distribution on nodes, edges, or faces of the 2D continuum FE model requires a lot of work. Therefore, in this study, a generalized form of the mode shape-dependent load offered by DIANA was adopted for NSA. This provides a load distribution over all elements that have a mass matrix. To use this load, a free vibration-type eigenvalue analysis was first performed. The results showed that the first mode was predominant for the considered frames PF4 and PF8. Hence, the six considered FE models of the structures were subjected to increasing first mode-shape-dependent lateral loads. The NSA was performed by referring to the previous work done by Chopra

and Goel [51]. Moreover, the NSA was conducted for a maximum drift ratio of 0.02 (2%); this corresponds to the life safety performance level described in ASCE 41 [24]. The results of the NSA were expressed as a normalized base shear versus "roof drift ratio," defined as the peak roof displacement divided by the height of the roof above the base. The base shear force (V_{base}) was obtained from the summation of the horizontal reaction forces at the base and normalized by the total seismic weight (W) of the structures.

Figure 8 depicts the relationships between the normalized base shear and roof drift ratio for all frames under the first mode-shape-dependent lateral loads. It should be noted that the undertaken analyses neglected geometric nonlinearities. Accordingly, the predicted base shear-roof drift curves do not allow for second-order ($P - \Delta$) effects, which are significant at large horizontal deflections. For Frame PF4-noJH, the analysis could not proceed up to the target drift because of numerical convergence issues. Hence, only the converged results are shown in Figure 8(a).

The results of the pushover analyses indicate that the maximum base shear strengths of frames PF4 and PF8 are $0.26\,W$ and $0.13\,W$, respectively, at a roof drift ratio of ~1%. For PF4-R and PF8-R, the maximum base shear was similar to that observed in the reference frames (PF4 and PF8). The rigid joint assumption did not noticeably affect the base shear strengths of PF4-R and PF8-R; however, PF4-R (the frame with rigid joints) exhibited a slightly larger lateral stiffness than those with flexible joints (i.e., PF4 and PF4-noJH). However, the first mode natural periods of the four-story frames were almost identical; these were determined as 0.62 s from the eigenvalue analysis. The difference in lateral stiffness was negligible between the eight-story frames, and their first-mode natural periods were predicted to be 1.16 s, regardless of joint flexibility.

Figure 9 shows the definition of flexural deformation of beams and columns determined from 2D continuum FE models, and Figure 10 illustrates the inelastic deformation distribution over the height of the reference structures (i.e., PF4 and PF8) as a representative example. Since the average curvature of critical sections of concrete structural members can be very important to accurately predict the overall deformation under serviceability conditions and to assess the ductility in ultimate limit states, the flexural deformation is expressed as the curvature of structural members (Figure 9(a)). Thus, the average curvature of beams and columns up to failure was evaluated at three distinct states: (1) the curvature corresponds to the initially uncracked section; (2) the curvature is associated with the entirely cracked section; and (3) the curvature corresponds to the steel yielding or concrete crushing. The joint shear stress and deformation were determined by averaging the values of the diagonal elements of the joint panel in the FE model, as depicted in Figure 9(b).

Moreover, for the reference frame PF4 (which well satisfies the minimum seismic requirements of the ACI 318-19 and ACI 352 codes), inelastic flexural deformation formed at the ends of the second- and third-story columns at a roof drift ratio of 2%. Consequently, the deformation characteristics of the structure changed significantly. This indicates that the structure tends to fail via a column-sway mechanism at higher drift ratios. In addition, the column-to-beam flexural strength ratio of 1.5, which is greater than the currently required minimum strength ratio of 1.2, is insufficient to prevent the formation of inelastic flexural deformation at the column ends across the stories. Therefore, the current strong-column, weak-beam design provision of ACI 318-19 delays but does not prevent column hinges and the formation of a story mechanism. Furthermore, the interior BC joints in PF4 suffered moderate damage with a drift ratio of 2% (Figure 10(a)). The corresponding joint shear deformation was ~0.007 rad. Note that these joints were designed according to ACI 318-19 and ACI 352.

Compared with PF4, Frame PF8 exhibited a beam-sway mechanism and no strength degradation; furthermore, the distribution of inelastic deformation across the stories was uniform at a drift ratio of 1%. Nevertheless, when the roof drift ratio increased further, the formation of plastic flexural deformations started at the top ends of the fifth- and sixth-story columns. Beams on the second, third, and fourth-floor levels sustained a significant amount of damage in both end sections. Moreover, the BC joints in this frame did not suffer any damage, and their behaviors were within the elastic range. Hence, these types of joints can be considered rigid.

5. Selected Earthquake Ground Motions

Six 2D FE models were subjected to actual earthquake ground motions extracted from the Pacific Earthquake Engineering Research (PEER) database [52]. In this work, seven ground motions were selected as base input motions because they are well-known motions that caused a significant damage to engineering structures in earthquake-affected areas. The selected ground motions depended on the purpose of the seismic assessment. Generally, three types of performance assessments are widely utilized: intensity, scenario, and risk-based [53]. This study is an intensity-based assessment since the responses of the considered frames and their components were computed for a specified ground shaking intensity. Therefore, intensity is one of the main selection criteria. Other criteria included the moment magnitude, the closest distance to a fault rupture, and frequency content. The seven records represent earthquakes with a magnitude M_w larger than 6.5, and the closest distance of the recording stations to a fault rupture is less than 15 km (near-fault). It should be noted that the selected records displayed near-fault rupture directivity effects.

The frequency content of the earthquake ground motion is crucial because it influences the dynamic responses of structural systems. A helpful parameter for characterizing the frequency content of earthquake motions is the so-called "A/v ratio." Here, A is the absolute peak ground acceleration (PGA) is expressed in units of gravitational acceleration, and v is the absolute peak ground velocity (PGV) is expressed in m/s. Following Tso et al. [54], earthquake ground motions were categorized into high-, medium-, and low-frequency ranges, depending on the value of the A/v ratio. Thus, $A/v > 1.2$ g/m/s was classified into the high range, whereas $A/v < 0.8$ g/m/s was categorized into the low one; $0.8\,g/m/s \leq A/v \leq 1.2\,g/m/s$

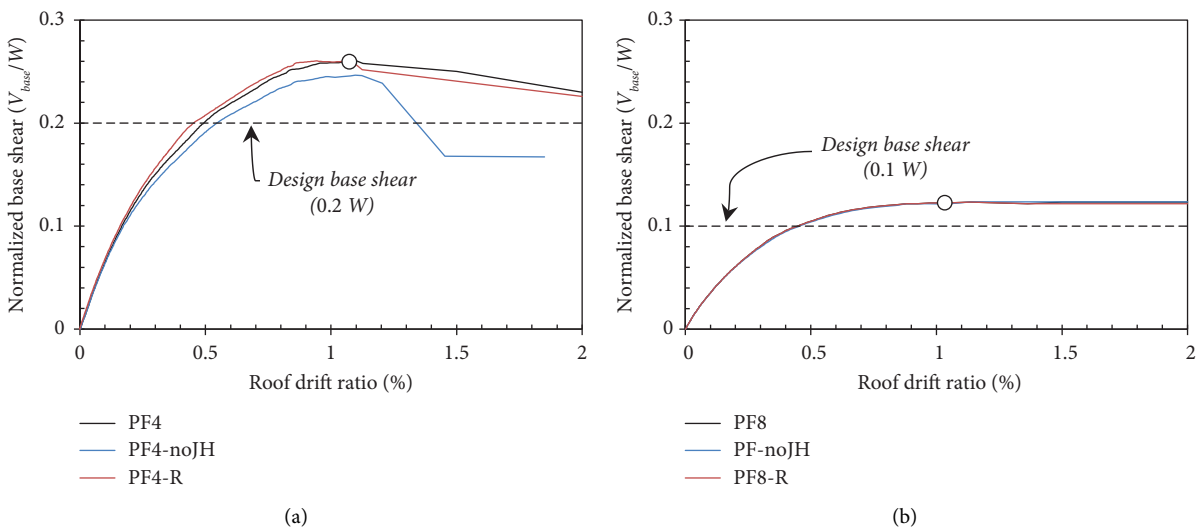

Figure 8: Pushover analysis results: normalized base shear with respect to roof drift ratio. (a) A four-story frame. (b) An eight-story frame.

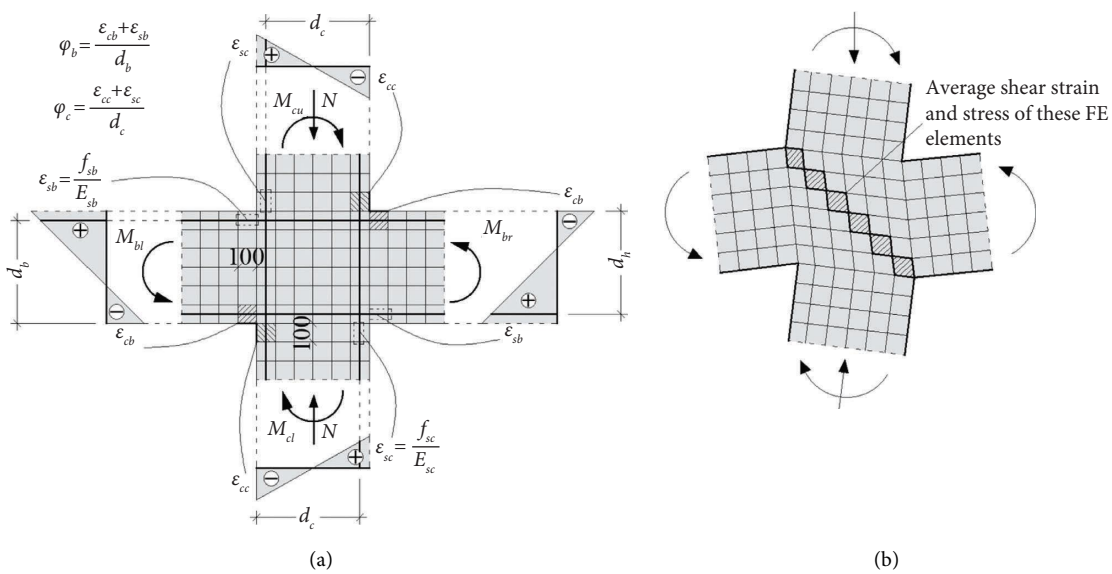

Figure 9: Determination of the deformation of structural members from 2D continuum FE models. (a) Flexural deformation of beams and columns. (b) Shear stress and deformation of joints.

denoted the medium range. The characteristics of these seven earthquakes are listed in Table 2. Figure 11 shows the acceleration response spectra of the base input motions.

6. Nonlinear Dynamic Analysis

The variation in the dynamic responses of the frames with different properties at the BC joints was investigated using nonlinear dynamic analysis. The FE models of all frames were subjected to the acceleration histories of the ground motions as presented in Table 2. Furthermore, gravity loads were applied to the beams of all stories as a uniformly distributed force. The magnitude of the applied force was 48 N/mm. The total seismic weights (W) of the four- and eight-story frames were allocated to Nodes 12 and 24, respectively, where the centerlines of the beams intersected with those of the columns, as illustrated in Figure 6(b). A point mass element (the red point in Figure 6(b)) was used to represent the lumped mass on each floor, and the mass value was 17.1 tons. Rayleigh damping was used to model the energy dissipation characteristics of the structure to capture the decay. The values of the mass- and stiffness-proportional damping parameters were chosen as 0.236 1/s and 0.00789 s, respectively, to produce a 5% critical damping in the first and second modes for a bare RC frame.

7. Analysis Results and Discussion

The results of the nonlinear dynamic analyses were examined and compared in terms of the global and local responses of the four- and eight-story frames to determine the effects of rigid and flexible joint modeling approaches (as well as joint

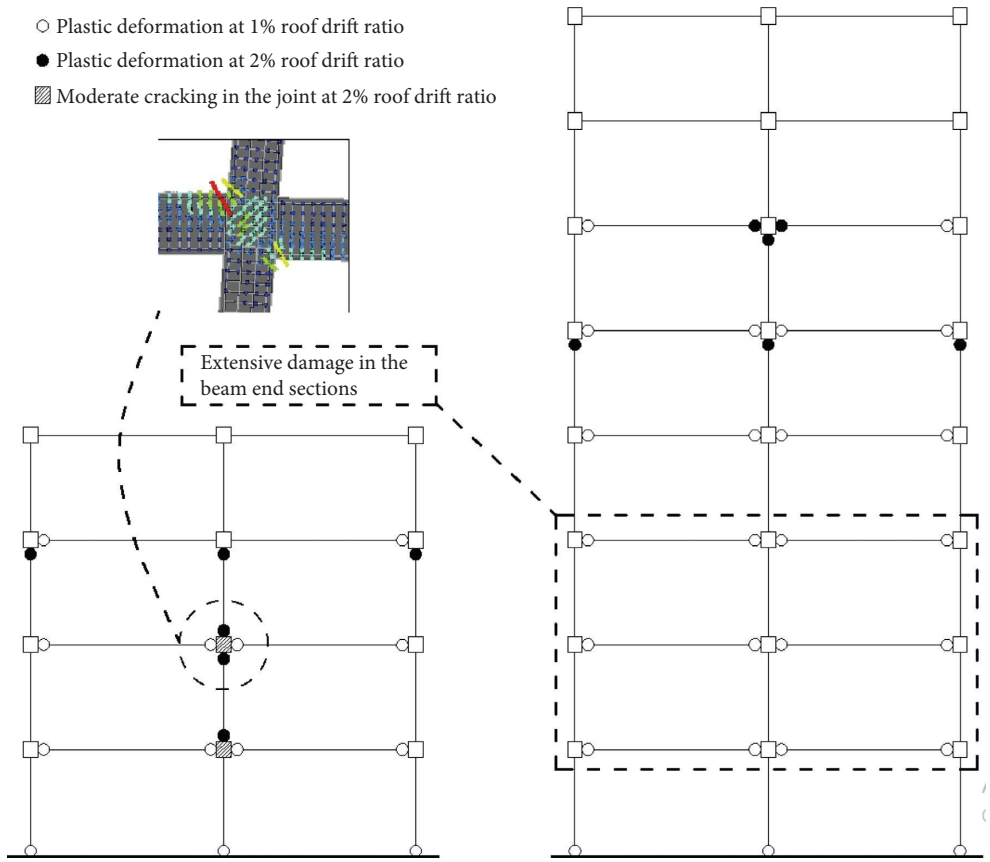

(a) (b)

Figure 10: Plastic deformation distribution over the height of the frame structures at two different roof drift ratios. (a) Reference frame "PF4." (b) Reference frame "PF8."

Table 2: Characteristics of the selected ground motions.

Record ID	Earthquake	M_w	Station	R_{rup} (km)	PGA (g)	PGV (m/s)	A/v ratio	Frequency content
1	El Centro 1940	6.95	El Centro array #9	6.09	0.28	0.31	0.91	Medium
2	Kobe 1995	6.9	KJMA	0.96	0.83	0.91	0.92	Medium
3	Loma Prieta 1989	6.93	BRAN	10.7	0.46	0.51	0.89	Medium
4	Northridge 1994	6.69	Pardee—SCE	7.46	0.56	0.76	0.74	Low
5	Northridge 1994	6.69	Rinaldi receiving sta	6.5	0.87	1.48	0.59	Low
6	Chi-Chi Taiwan 1999	7.62	TCU071	0.32	0.53	0.52	1.02	Medium
7	Chi-Chi Taiwan 1999	7.62	TCU068	5.8	0.37	2.64	0.14	Low

M_w is the moment magnitude, and R_{rup} is the closest distance to a fault rupture. The effective durations of the ground motions are determined using the arias intensity measure I_A, which indicates the amount of energy expended in the production of damage.

shear reinforcement) on their seismic responses. The global response was studied in the form of curves describing the maximum transient interstory drift ratio (IDR) and hysteretic behavior (base shear versus roof drift). In addition, the local response was studied for the joint shear stress, joint shear deformation, and curvature of critical sections of the beam and column.

7.1. Global Responses of the Frames. As examples of the results, Figure 12 shows the distribution of maximum IDR over the height of the four- and eight-story frames subjected to two ground motions with PGAs of 0.83 g and 0.87 g (Record ID: 2 and ID: 5). The related hysteretic base shear-roof drift curves are shown in Figure 13. Interstory drift is defined as the difference in the displacements of adjacent floors, and it is often normalized with respect to the story height to obtain a nondimensional index of story deformation. The story deformation of the frames was assessed using the interstory limits defined by ASCE 41, in which the IDR of the RC moment frames should be at least 4% for collapse prevention, 2% for life safety, and 1% for immediate occupancy. The maximum IDR curves for Frames PF4-noJH and PF8-noJH are omitted in Figure 12 because of the

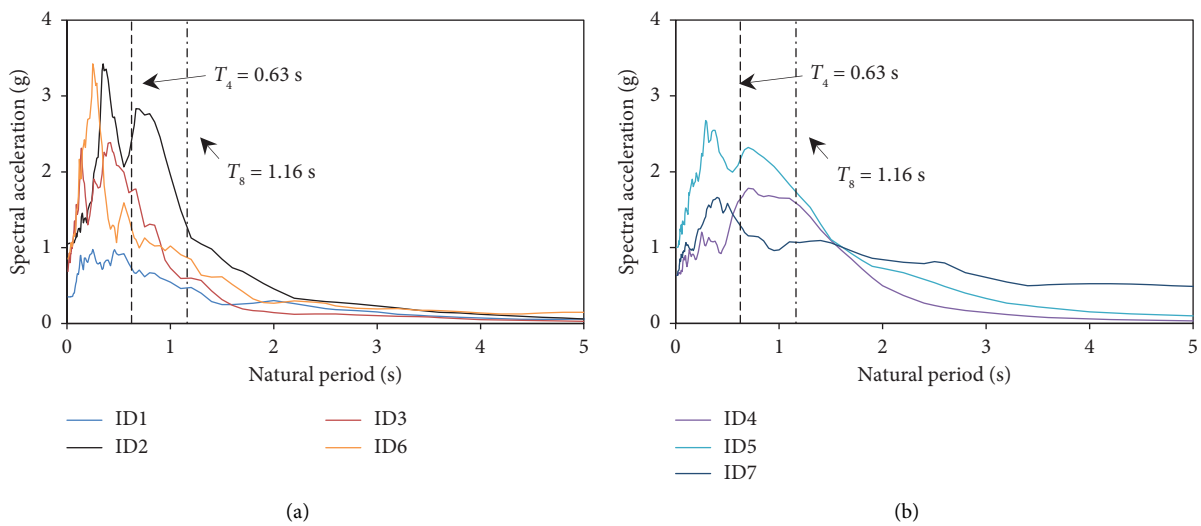

Figure 11: Response acceleration spectra of base input motions. (a) Earthquake motions in the medium-frequency range. (b) Earthquake motions in the low-frequency range.

marginal difference in drift values compared to PF4 and PF8. The predicted seismic demands are summarized in Tables 3 and 4 for the rigid and flexible modeling approaches, respectively. In Tables 3 and 4, the contribution of joint shear deformation to interstory drift is expressed as a joint shear deformation index (SDI) proposed by the authors [23]. SDI values of less than 0.2 indicate that the joint deformations do not contribute excessively to the overall story drift and that damage is expected in the beam end region, where they form a plastic hinge mechanism. Conversely, damage is expected both in the beam critical region and joint region if the SDI values are significantly greater than 0.2.

As shown in Figure 12, the lateral deflection of the four-story frames is primarily concentrated at the second- and third-floor levels for all selected input motions. In contrast, the deflections at the fourth- and fifth-floor levels are typically the largest for the eight-story frames. The lateral deformations at these levels are highlighted in the following sections. Figure 12(a) and Table 3 show that the maximum interstory drifts of the PF4-R differ from those of the PF4 (frame with flexible joints) by ~3–30% for the selected input base motions. More specifically, the difference was more pronounced during the Kobe earthquake ground motions (ID: 2). Moreover, the SDI values of the interior joint at the third-floor level of PF4 were 0.32 and 0.45 for Records ID: 2 and ID: 5, respectively. This implies that some damage occurred in the joint designed to satisfy the ACI 318-19 requirements. Furthermore, the SDI values for PF4-noJH were 20–30% larger than those observed in the PF4 frame.

Regarding the Northridge earthquake (ID: 5), a relatively small difference was observed in the drift of each story between PF4 and PF4-R, although the PGA exceeded that of the Kobe earthquake. This was attributable to the large plastic deformations imposed on the bottom of the first-story columns compared to those caused by the Kobe earthquake (Figure 12). Thus, the primary source of structural flexibility is the plastic rotation of the bottom ends of the first-story column. In general, the difference in interstory drift is attributed to the cracking of the joint panels, which increases the shear deformation of the joints (or SDI value). In contrast, the magnitude of the difference in the drift of each story between PF8 and PF8-R under different earthquake motions was comparatively small because the interior joints showed SDI values of less than 0.2 and did not suffer any significant cracking (Table 4). This smaller SDI was partly attributed to the larger column-to-beam flexural strength and column-to-beam area ratios for Frame PF8.

The selected ground motions imposed much higher seismic demands on the four-story structures than on the eight-story structures because of the shorter natural period (refer to Figure 11). As a result, the hysteretic behaviors and maximum base shears of the four-story structures differed considerably from those of the eight-story ones (Figure 13). In general, the maximum base shear demand obtained from the models with flexible joints resembled that of the models with rigid joints, as shown in Figure 13 and Tables 3 and 4. The maximum roof displacement demand in the four-story models with flexible joints differed from their counterparts (predicted under the assumption of rigid joint behavior) by an amount of the order of 2–35% (Figure 13(a) and Table 3). The magnitude of the difference in roof drift between Frames PF4 and PF4-R becomes very small for earthquake records with lower intensities (i.e., ID: 1, ID: 3, ID: 4, and ID: 6). Also, it should be mentioned here that the maximum base shears obtained from the nonlinear dynamic analyses for PF4 and PF8 were much greater than the design lateral force levels of 0.2 W and 0.1 W, respectively. This phenomenon was also observed in the experimental study conducted by Nagae et al. [17]. The inverted triangular lateral load distribution was used to design the structures. However, the vertical distribution of the lateral inertial forces was transformed into a nearly uniform distribution over the height of the structures due to large inelastic deformations in the

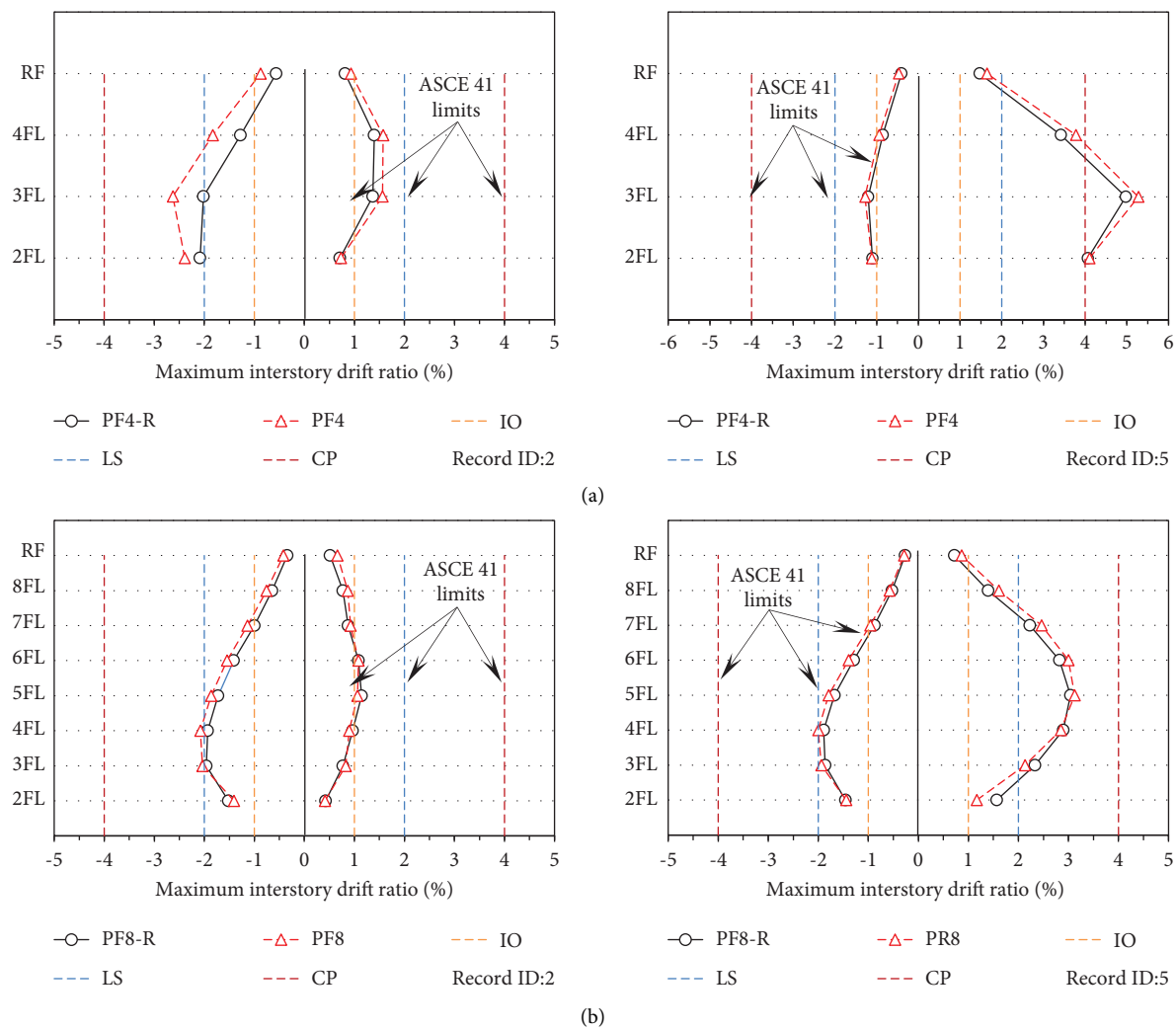

Figure 12: Maximum transient interstory drift ratio of each story. (a) A four-story frame. (b) An eight-story frame.

columns and interior joints of the first and second stories. This was one of the main reasons for the double increase in the base shear of these frames. Moreover, other factors (i.e., overstrength of materials, redundancy of the structural system, and nonlinear hysteretic damping) may have resulted in a significant increase in the maximum base shear during the dynamic analysis.

7.2. Local Response of the Frames. The seismic demands upon the individual structural members (e.g., interior and exterior joints, beams, and columns) of the four- and eight-story frames were evaluated to determine the effects of different joint modeling assumptions. The predicted demands included the joint shear deformation, joint shear stress, and curvatures of the beam and column end sections. The joint shear stress and deformation were evaluated from the 2D continuum FE analysis by following the same procedure described in Section 4 (refer to Figure 9(b)). Subsequently, the shear stress was normalized relative to the square root of the concrete's compressive strength. The curvatures of the beam and column end sections were defined as the ratio of the difference between the strains on the top and bottom extreme fibers of the sections and the distance between the fibers, as described in Section 4 (refer to Figure 9(a)). For consistency with the global response, the results from the Kobe and Northridge earthquakes (ID: 2 and ID: 5) were selected and illustrated in Figures 14–19. The absolute maximum values of both the shear stress and shear strain induced in the joints of the frames are presented in Table 5 for all ground motions.

7.2.1. Beam-Column Joint Response. Figures 14(a) and 14(b) depict the shear deformation time histories of the interior BC joint at the third-floor level of the PF4 and fifth-floor level of the PF8. The corresponding interstory drift of each frame is also superimposed in these figures because both drift and shear deformation have been measured in radians. In alignment with the previous experimental and analytical results [22, 23, 32], any joint with a joint shear deformation value greater than 0.02 rad was extensively damaged, irrespective of joint shear reinforcement quantity. It was also experimentally observed that joints with a shear deformation

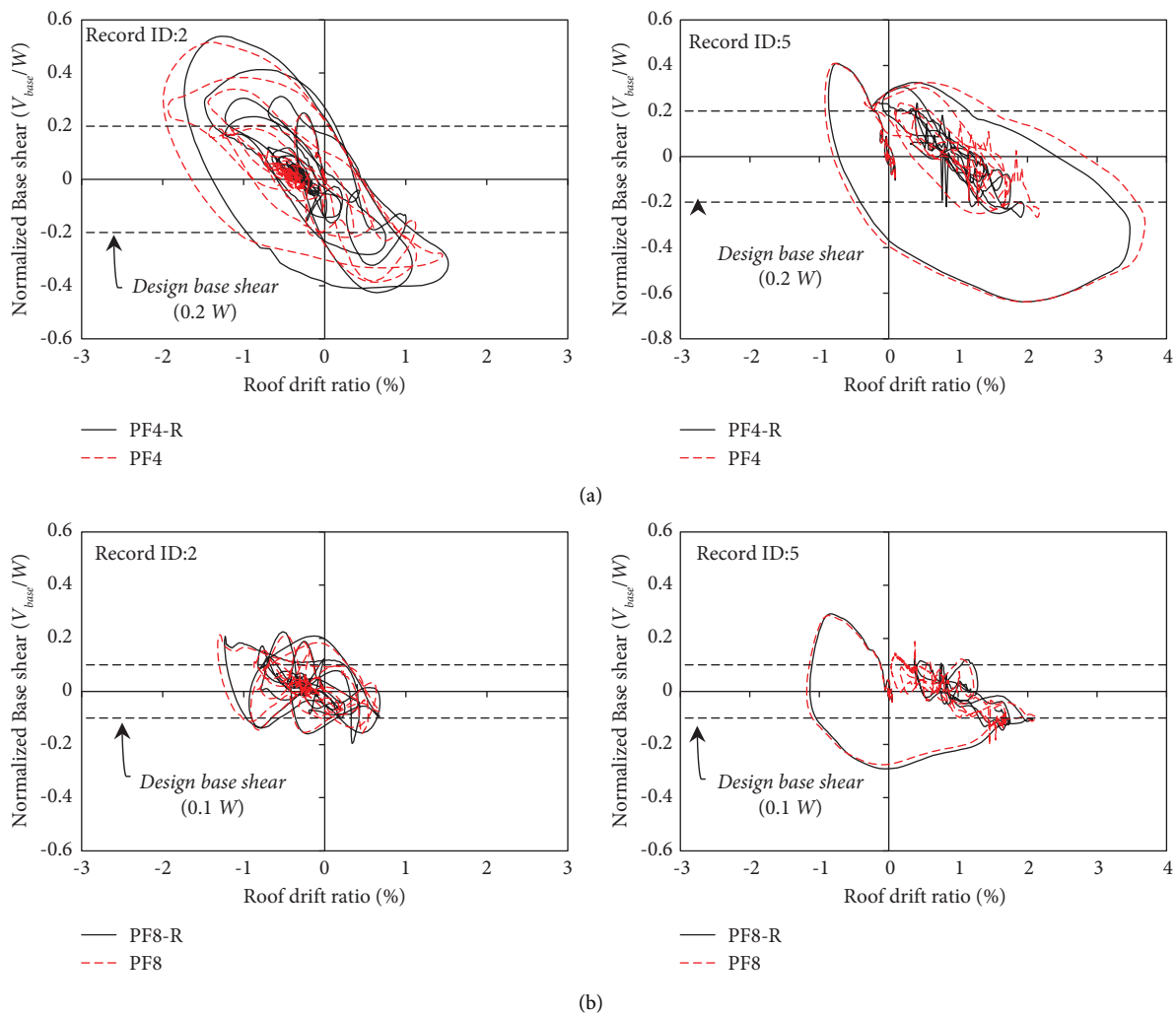

Figure 13: Hysteretic behavior and base shear demand. (a) A four-story frame. (b) An eight-story frame.

Table 3: Seismic demands placed upon the four-story frames for the selected ground motions.

Record ID	Maximum roof drift ratio (%)			Maximum normalized base shear (V_{base}/W)			Maximum IDR at 3FL level (%)			Maximum SDI of interior joint at 3FL level		
	PF4	PF4-noJH	PF4-R	PF4	PF4-noJH	PF4-R	PF4	PF4-noJH	PF4-R	PF4	PF4-noJH	PF4-R
1	0.51	0.51	0.50	0.25	0.24	0.26	0.69	0.68	0.67	0.15	0.20	—
2	1.99	1.99	1.48	0.52	0.51	0.54	2.63	2.62	2.01	0.32	0.39	—
3	0.84	0.83	0.81	0.34	0.34	0.35	1.12	1.10	1.00	0.18	0.21	—
4	2.14	2.12	—	0.48	0.47	—	3.02	2.99	—	0.23	0.27	—
5	3.69	3.69	3.47	0.64	0.63	0.69	5.28	5.27	4.97	0.45	0.46	—
6	0.81	0.81	0.79	0.34	0.35	0.34	1.09	1.09	1.06	0.17	0.20	—
7	1.05	1.05	0.91	0.37	0.37	0.40	1.43	1.43	1.23	0.19	0.28	—

of 0.010.02 rad suffered a significant amount of diagonal cracking. Within this range, the joints exhibited their maximum shear strengths. The yielding deformation of joints usually starts at 0.005–0.01 rad, depending on the extent of joint transverse reinforcement. In this range, joints suffer a moderate amount of diagonal cracking with smaller widths. Diagonal cracking usually forms in joints at a shear strain value of ~0.00025 rad. Based on the above information and the distributions and widths of diagonal cracks in the joints (as predicted by the 2D continuum FE analysis), the damage levels of the BC joints were determined. In general, it is believed that well-designed BC joints (i.e., those meeting the provisions of the current seismic design codes) are expected to have a maximum shear deformation of approximately 0.005 rad or less [17, 20, 23, and 29]. This shear deformation value corresponds to an SDI value of 0.2 or less.

In the present work, the joint shear deformation did not exceed the value of 0.02 rad for either the four- or

Table 4: Seismic demands placed upon the eight-story frames for the selected ground motions.

Record ID	Maximum roof drift ratio (%)			Maximum normalized base shear (V_{base}/W)			Maximum IDR at 5FL level (%)			Maximum SDI of interior joint at 5FL level		
	PF8	PF8-noJH	PF8-R	PF8	PF8-noJH	PF8-R	PF8	PF8-noJH	PF8-R	PF8	PF8-noJH	PF8-R
1	0.64	0.64	—	0.16	0.16	—	0.90	0.91	—	0.06	0.07	—
2	1.32	1.28	1.24	0.21	0.21	0.22	1.86	1.77	1.72	0.11	0.18	—
3	0.55	0.55	—	0.18	0.17	—	0.83	0.83	—	0.06	0.06	—
4	1.08	1.08	—	0.23	0.23	—	1.68	1.68	—	0.10	0.10	—
5	2.12	2.12	2.07	0.29	0.29	0.29	3.13	3.13	3.04	0.08	0.11	—
6	0.78	0.77	—	0.22	0.21	—	1.24	1.23	—	0.08	0.08	—
7	2.83	2.85	—	0.23	0.23	—	3.84	3.86	—	0.07	0.11	—

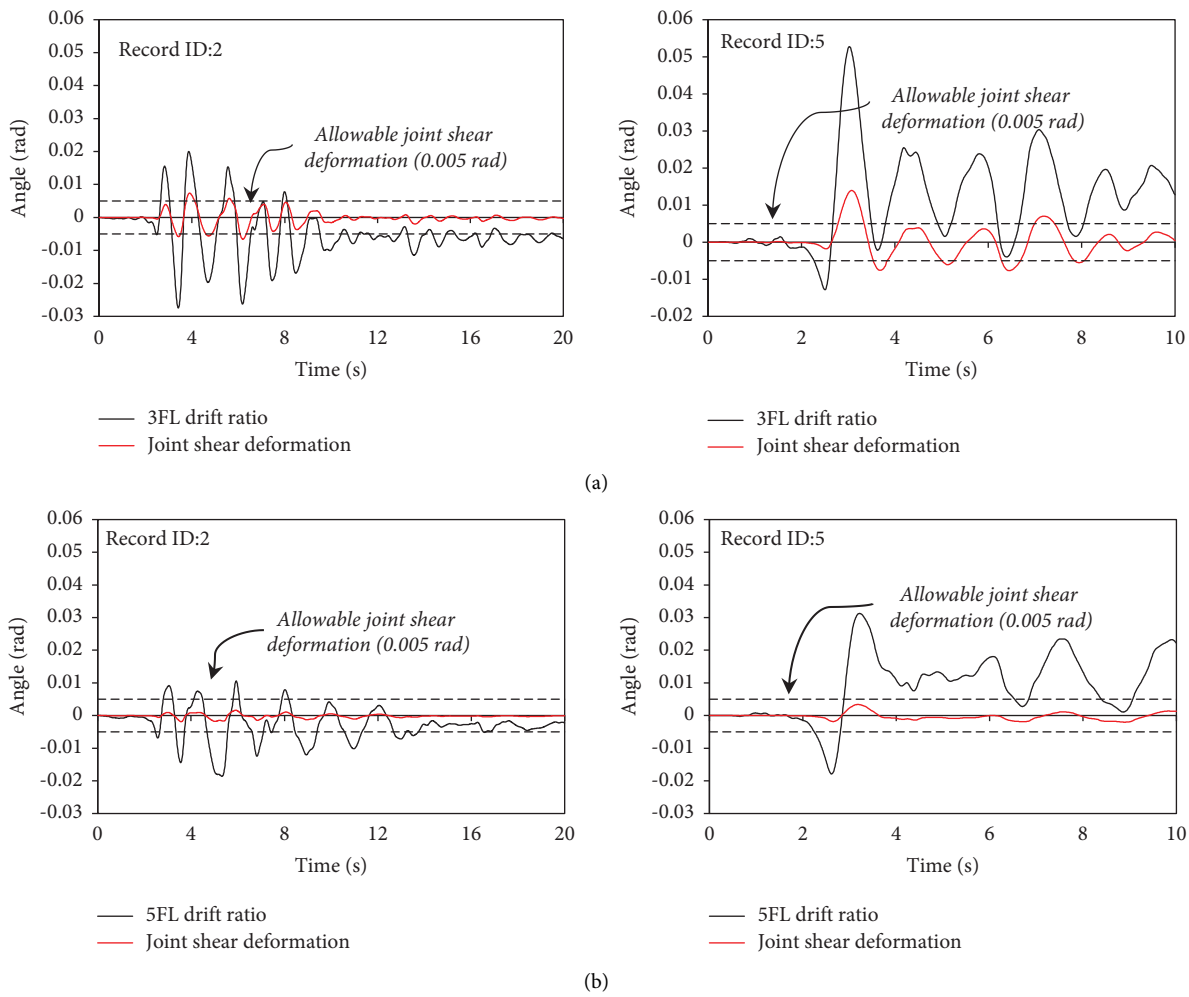

Figure 14: Joint shear deformation history. (a) Frame PF4: interior joint at 3 FL. (b) Frame PF8: interior joint at 5 FL.

eight-story FE models, including the models without joint shear reinforcement. As shown in Figures 14(a) and 14(b), the maximum shear deformations of the selected interior joint in Frame PF4 were approximately three and four times higher than that of the interior joint in Frame PF8 for the Kobe and Northridge earthquakes, respectively. Accordingly, larger diagonal cracks appeared in the PF4 joint compared with the PF8 one. In general, the interior joints of the four-story structure exhibited significant damage for Record ID: 5 and light-to-moderate damage for the other records (Table 5). However, small diagonal cracks appeared in the interior joint of PF8 for Records ID: 1–4 and ID: 7, and the joint suffered light damage for Records ID: 5 and ID: 6. The interior joints in Frames PF4-noJH and PF8-noJH displayed shear deformation at a maximum of ~23% higher than that observed in their counterparts with shear reinforcement. As shown in Table 5, comparatively less variation was observed in the joint shear stress than in joint shear deformation. The maximum shear stress demands on the interior joints for Frames PF4

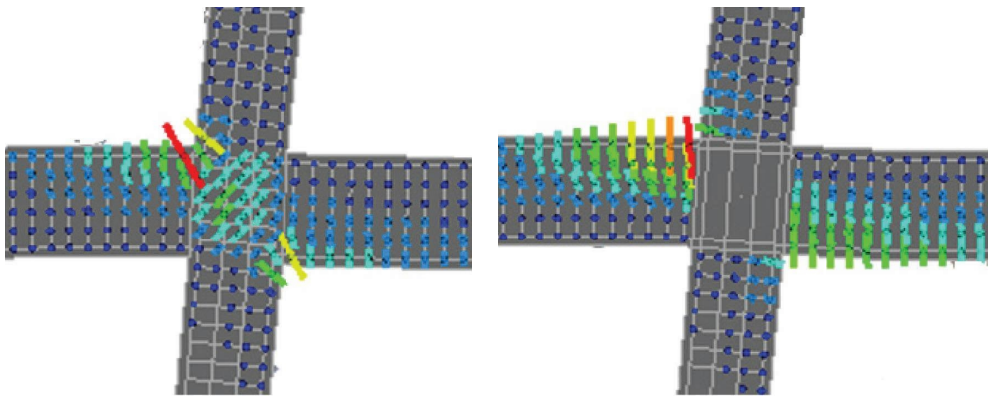

(a) (b)

Figure 15: Crack distribution in structural members at the BC joint for the peak ground acceleration of record ID: 5 ($t = 3.01$ sec). (a) Frame PF4: interior joint at 3 FL level. (b) Frame PF4-R: interior joint at 3 FL level.

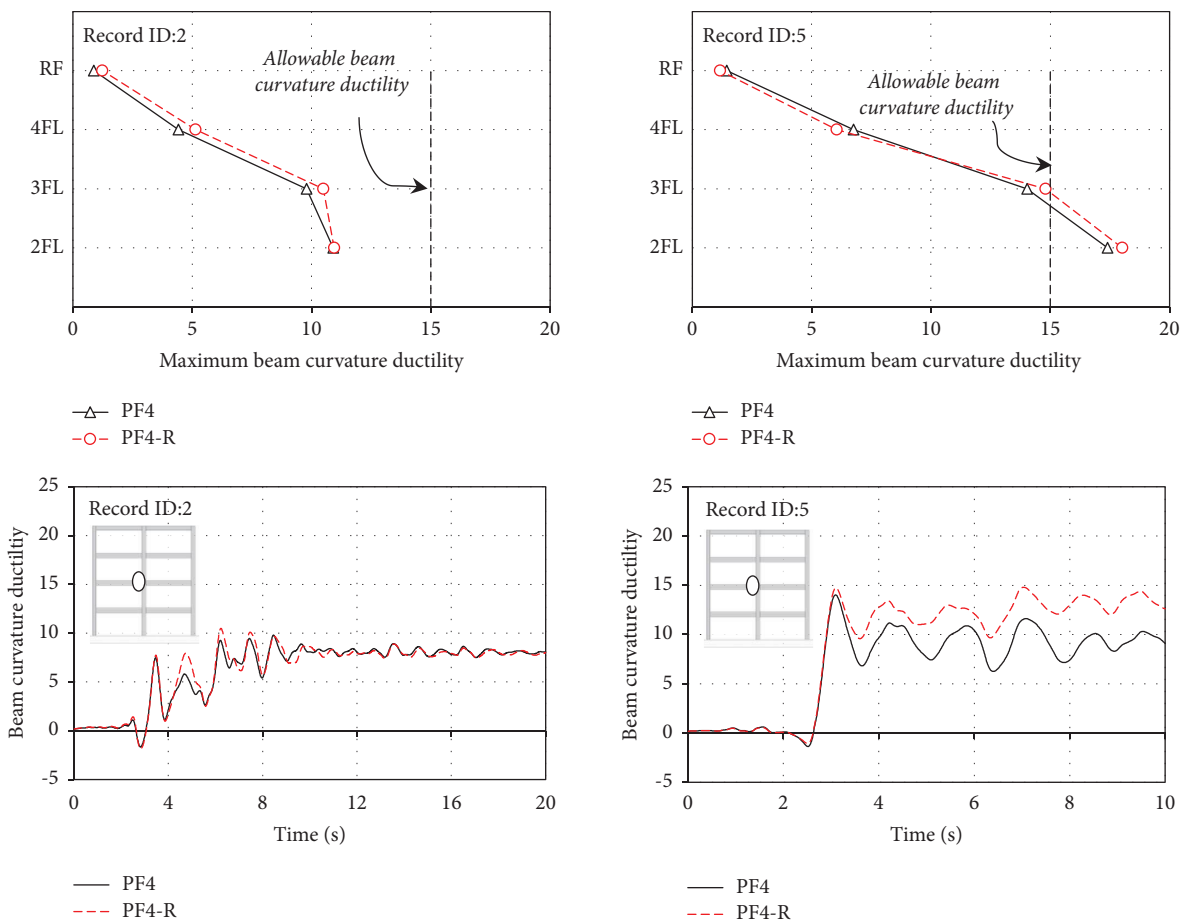

Figure 16: Maximum curvature ductility demands placed upon the beams of the four-story frames subjected to Kobe and Northridge earthquake ground motions.

and PF8 were 1.4 $\sqrt{f'_c}$ and 1.19 $\sqrt{f'_c}$, respectively. Although the shear demand exceeded the shear strength of the joint by an order of 5–12%, the damage was not so severe in the joint region.

As an example, Figure 15 shows the crack distributions of the interior BC joint connections at the third-floor level of Frames PF4 and PF4-R subjected to ground motion with 0.87 g (Record ID: 5). The crack propagation in beams and columns varied with respect to the joint modeling approaches. For the model with a rigid joint, a significant amount of cracking in the beam end sections was observed, and the depth of the cracks was not as shallow as that observed in the model with a flexible joint. When the cracking was allowed in the joint region, the

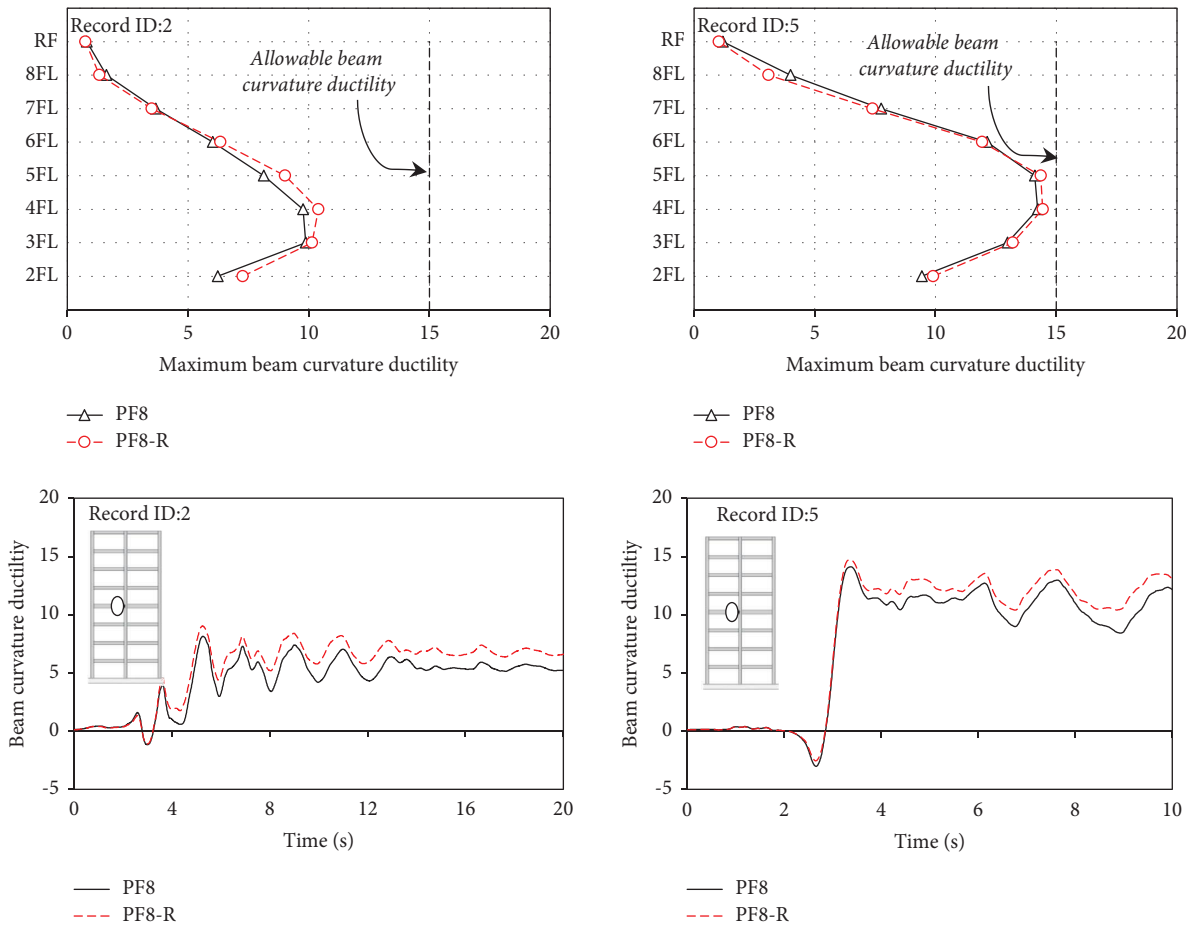

Figure 17: Maximum curvature ductility demands placed upon the beams of the eight-story frames subjected to Kobe and Northridge earthquake ground motions.

width and prorogation of the cracks became larger in the column end sections. This implies that the inelastic deformation formed at the ends of the second- and third-story columns.

The joint shear deformation was significantly smaller in the exterior joints, as shown in Table 5. For all records, the formation of diagonal cracks started in the exterior joint at the 3 FL level of PF4, whereas relatively small cracking occurred in the exterior joint of PF8 during these two earthquakes. Hence, the contribution of exterior joint deformation to story drift was relatively small. This was attributed to the larger column-to-beam flexural strength ratio and the lower shear stress level in the joint. However, this statement does not always hold true since the steel reinforcement was simplified in the FE model by neglecting the inclined portions of the steel bars present in the exterior BC joints. In addition, the actual bond strength between the concrete and steel reinforcement was neglected in this study.

7.2.2. Beam and Column Responses. In response of a moment-resisting frame to an earthquake, the curvature ductility of the sections of structural members is essential to preventing brittle failure of the structure by ensuring adequate curvature at the ultimate limit state. Therefore, it may be more convenient to evaluate the ductility of members using the definition of curvature ductility. To verify the results of the analyses, the limiting values of the curvature ductility for ductile beams and columns were taken as 15 and 20, respectively. These values are generally the average values specified by seismic provisions in concrete design codes [7, 8] according to the experimental database.

Figures 16–19 show the predicted curvature ductility demands on the beams and columns of the four- and eight-story frames subjected to the ground motions of Records ID: 2 and ID: 5. It can be seen that Record ID: 5 caused the structures to develop much higher curvature ductility in beams and columns in comparison to Record ID: 2, despite the subtle difference in PGA. For instance, the maximum curvature ductility in the beams of the first story for PF4 was 17.4 for Record ID: 5, whereas the ductility value was predicted to be 10.9 for Record ID: 2. The maximum curvature ductility demands for the first story column of the PF4 were found to be 9.01 and 15.0 for Records ID: 2 and ID: 5, respectively. These results indicate that an earthquake with low-frequency content (ID: 5) is more detrimental to the structures in that situation. Furthermore, a similar tendency was observed in the results obtained from other seismic response analyses.

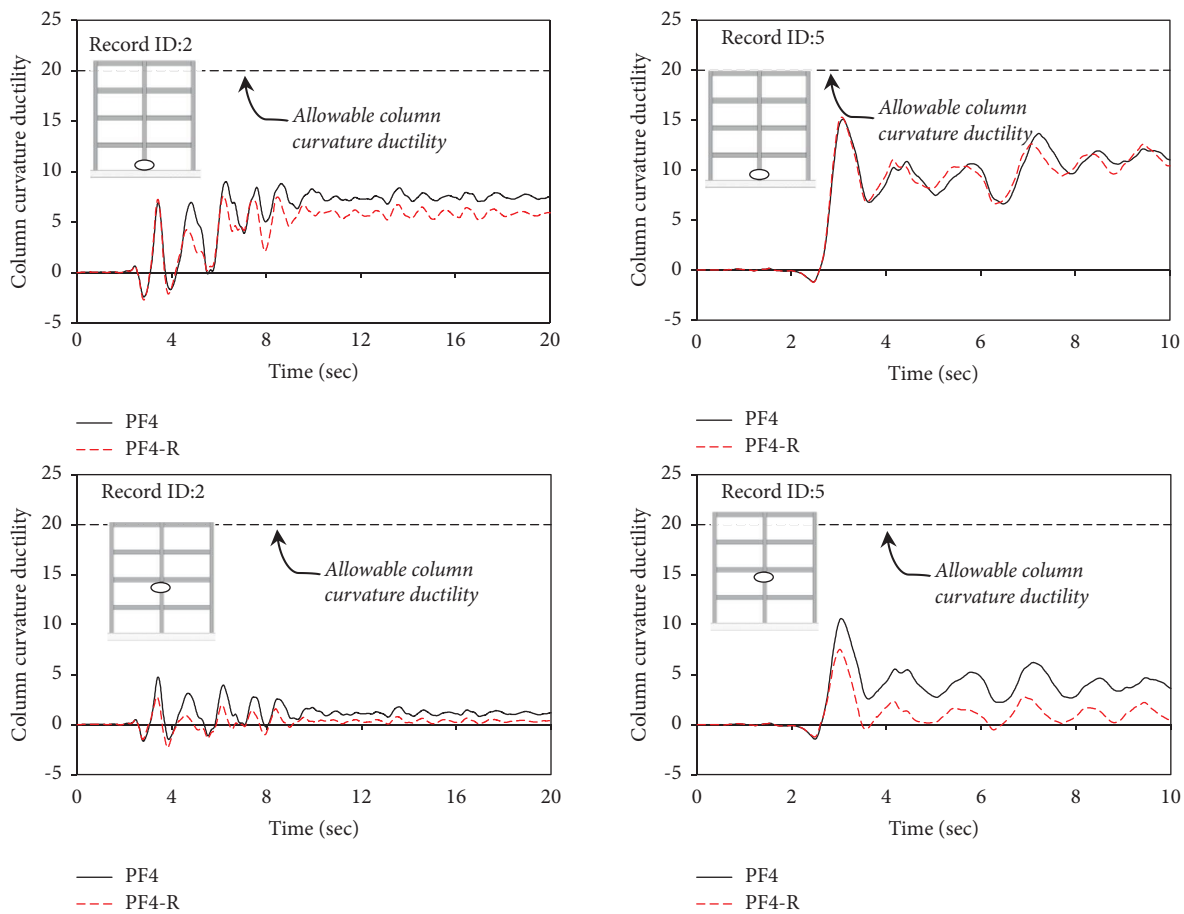

Figure 18: Time histories of curvature ductility demand placed upon the columns of the four-story frames subjected to Kobe and Northridge earthquake ground motions.

A comparison between the models with rigid and flexible joints shows that the ductility demands on the beams and columns varied with respect to the joint modeling approaches. The models with flexible joints generally exhibited 5–8% lower ductility demands in the beams than those with rigid joints at levels where high joint shear deformations occurred. Consequently, the residual deformations in the beams were slightly larger for Frames PF4-R and PF8-R (Figures 16 and 17, respectively). This scenario is reversed for the columns of the intermediate stories, where joint deformations are large. For Frame PF4 subjected to the Kobe earthquake motion, the curvature ductility demand on the interior column of the second story increased by 68% compared to that of Frame PF4-R, for which cracking did not form within the joint region (Figure 18). The difference in demand was 41% for the Northridge earthquake. The results indicate that the curvature ductility demand on the columns is likely to exceed that predicted by the FE models under the rigid joint assumption; this emphasizes the importance of considering joint cracking on the seismic response of the beams and columns framing the joint.

Regarding the eight-story frames under two strong seismic attacks, the maximum curvature ductility demands on the interior column of the fourth story (where the largest interstory drifts and joint shear deformations occurred) were relatively small compared to the four-story frames. As shown in Figure 19, flexural yielding did not occur in the interior column of the fourth story of Frames PF8 and PF8-R subjected to the Kobe earthquake. No significant differences in column responses were found between them. In the case of the Northridge earthquake, the selected interior columns of Frames PF8 and PF8-R yielded demand values of 2.63 and 2.32, respectively. A small difference in the curvature ductility demand was observed on the selected interior columns between Frames PF8 and PF8-R for the Northridge earthquake, as shown in Figure 19. According to the results of other dynamic analyses, the effect of joint cracking was found to be significant in the four-story structure. This implies that the actual seismic demand for the columns in structures under strong seismic attacks is underestimated by a maximum of ~70% of that predicted by the structural analysis under the assumption of rigid joints. Hence, joints designed to satisfy

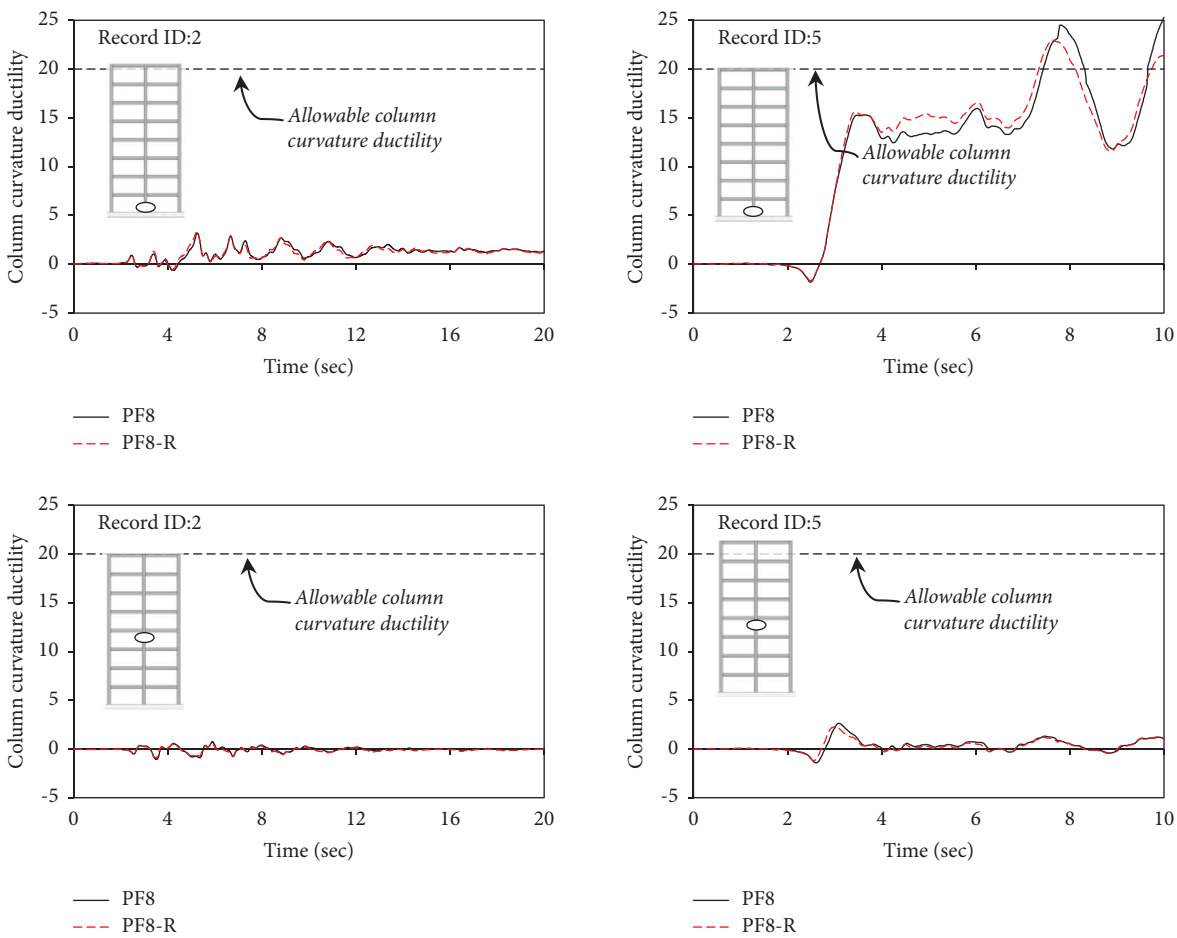

Figure 19: Time histories of curvature ductility demand placed upon the columns of the eight-story frames subjected to Kobe and Northridge earthquake ground motions.

Table 5: Seismic demands placed upon the interior and exterior joints of the considered frames for the selected ground motions.

Record ID	Interior joint								Exterior joint			
	Maximum shear deformation (rad)				Maximum shear stress $(v_j/\sqrt{f'_c})$				Maximum shear deformation (rad)		Maximum shear stress $(v_j/\sqrt{f'_c})$	
	3 FL PF4	3 FL PF4-noJH	5 FL PF8	5 FL PF8-noJH	3 FL PF4	3 FL PF4-noJH	5 FL PF8	5 FL PF8-noJH	3 FL PF4	5 FL PF8	3 FL PF4	5 FL PF8
1	0.0013	0.0016	0.0006	0.0006	0.89	0.85	0.53	0.55	0.0009	—	0.53	—
2	0.0066	0.0082	0.0018	0.0029	1.40	1.37	0.90	0.88	0.0027	0.0007	0.85	0.29
3	0.0026	0.0030	0.0007	0.0007	1.32	1.29	0.70	0.72	0.0013	—	0.64	—
4	0.0090	0.0106	0.0020	0.0021	1.36	1.20	1.12	1.12	0.0023	—	0.99	—
5	0.0139	0.0151	0.0034	0.0057	1.36	1.30	1.19	1.18	0.0035	0.0010	0.99	0.58
6	0.0031	0.0043	0.0033	0.0047	1.30	1.28	1.16	1.13	0.0017	—	0.74	—
7	0.0025	0.0029	0.0011	0.0013	1.19	1.18	0.85	0.86	0.0010	—	0.59	—

For the exterior joint in PF8, only results from records 2 and 5 are included because they are the largest. Furthermore, the seismic demands obtained from records 1, 2–4, and 5-6 are minimal, and the inclusion of these results is considered insignificant.

modern code requirements cannot always be considered sufficiently rigid when the column-to-beam flexural strength ratio and column-to-beam area ratio are less than 1.5.

8. Conclusions

In this study, nonlinear static and dynamic analyses were conducted to investigate the effect of the flexibility of joints (designed to meet modern code requirements) on the expected performance of low- to midrise RC MRF structures designed and constructed according to modern building code provisions; such joints are often assumed to exhibit no flexibility in seismic research. Six 2D continuum FE models of four- and eight-story frames (with rigid and flexible joints) were constructed and analyzed. Based on the results obtained from the analyses, the following conclusions can be drawn:

(i) The four- and eight-story FE models with flexible joints (excluding the four-story model without joint shear reinforcement) exhibited the same pushover curves as their counterparts with rigid joints. In addition, the rigid joint assumption did not affect the natural periods of the structures. The pushover results indicate that the four-story structure would fail via the column-sway mechanism, whereas the eight-story structure would fail via the beam-sway mechanism. The column-to-beam flexural strength ratio of 1.5, which is greater than the currently required minimum strength ratio of 1.2, is insufficient to prevent the columns from yielding. Therefore, the current strong-column, weak-beam design provision of ACI 318-19 delays but does not prevent column hinges and the formation of a story mechanism.

(ii) In contrast to the static behavior, the dynamic behaviors of models with flexible joints differed from those of models with rigid joints for the seven selected earthquakes. This difference was attributable to the joint deformations over the heights of the four- and eight-story frames. The magnitude of the difference in behavior depends on the characteristics of the earthquake (e.g., PGA, PGV, and frequency content). The seismic demands on frames vary in relation to the joint modeling approaches. In particular, the change in demand was relatively large for the four-story structure, owing to two factors. First, the structure had smaller ratios of column-to-beam flexural strength and column-to-beam area compared with the eight-story one. Second, the natural period of the four-story structure lies within the range of higher spectral accelerations for the selected input motions.

(iii) Concerning the global responses of the structures, the four- and eight-story FE models with flexible joints exhibited the same hysteretic behaviors and base shear strengths as their counterparts with rigid joints. However, from the deformation point of view, the four-story model with flexible joints had larger lateral deformation due to excessive inelastic deformation in the interior joints and columns in the first and second stories. This can result in the frame losing lateral and gravity load-carrying capacity. For the eight-story model, the discrepancies were negligible.

(iv) Regarding the joint response, the maximum joint shear deformation was observed in the interior joints of the middle floors of the four- and eight-story frames. The maximum joint shear deformation observed in the four-story model was ~3-4 times higher than that observed in the eight-story model. Accordingly, the interior joints in the middle floors of the four-story frame suffered light to moderate damage from the selected ground motions. In the eight-story frame, damage generally did not occur in the interior joints. The maximum shear stress demands on the interior joints for the four- and eight-story frames were 1.4 $\sqrt{f'_c}$ and 1.19 $\sqrt{f'_c}$, respectively. Although the shear demand exceeded the shear strength of the joint by an order of 5–12%, damage to the joints was not severe.

(v) The seismic demands of the beams and columns were affected by different joint modeling approaches. The models with flexible joints generally exhibited 5–8% lower curvature ductility demand in the beams than those with rigid joints at levels where high joint shear deformations occurred. In contrast, the curvature ductility demand for the columns in the four-story structure under strong ground motions was underestimated by a maximum of ~70% of that predicted by the structural analysis under the assumption of rigid joints. Hence, joints designed to satisfy modern code requirements cannot always be considered sufficiently rigid when the column-to-beam flexural strength ratio and column-to-beam area ratio are less than 1.5.

In this study, the lateral deformation of the frames attributable to slippage of the bars is not considered. Hence, the effect of the lap-splice and anchorage details of the beam bars within the joint region on the seismic performance is neglected. Also, the SSI effect is not taken into account. Despite these simplifications, the results obtained from this study indicate that practical structural analysis based on the assumption of rigid joints predicts structural behaviors (i.e., the deformation demand and the magnitude of the internal actions) that deviate significantly from those predicted when assuming elastic material properties for the joint regions. This study can be extended by considering the bond-slip behavior of reinforcing bars, the SSI effect, and the mass and/or stiffness irregularities to obtain a better understanding of the seismic performance of modern RC-framed buildings.

Data Availability

The data for different strong earthquakes is available from the Pacific Earthquake Engineering Research Center (PEER) web site.

Conflicts of Interest

The authors declare that they have no conflicts of interest.

References

[1] H. Sezen, K. J. Elwood, A. S. Whittaker, K. M. Mosalam, J. W. Wallace, and J. F. Stanton, "Structural engineering reconnaissance of the august 17, 1999, kocaeli (izmit), Turkey, earthquake," University of California, Berkeley, CA, USA, PEER 2000/09, 2000.

[2] M. S. Günay and K. M. Mosalam, "Structural engineering reconnaissance of the april 6, 2009, abruzzo, Italy, earthquake, and lessons learned," University of California, Berkeley, CA, USA, PEER 2010/105, 2010.

[3] T. Paulay and M. J. N. Priestley, *Seismic Design of Reinforced concrete and Masonry Buildings*, John Wiley & Sons, New York, NY, USA, 1992.

[4] G. Penelis and G. Penelis, *Concrete Buildings in Seismic Regions*, Taylor & Francis Group, Boca Raton, FL, USA, 2014.

[5] Aci Committee 318, *Building Code Requirements for Structural Concrete (ACI 318-19) Commentary on Building Code Requirements for Structural Concrete (ACI 318R-19)*, p. 443, American Concrete Institute, Farmington Hills, MI, USA, 2019.

[6] Architectural Institute of Japan, *AIJ Standard for Structural Calculation of Reinforced concrete Structures*, Architectural Institute of Japan, Tokyo, Japan, 2014.

[7] Standards New Zealand, *Concrete Structures Standard - the Design of Concrete Structures; NZS3101-1:2006*, Vol. 1, Standards New Zealand, , Wellington, New Zealand, 2006.

[8] European Commitee for Standardization, "Eurocode 8: design of structures for earthquake resistance-part 1: general rules, seismic actions and rules for buildings," *Eur Comm Stand*, vol. 1, p. 231, 2004.

[9] T. Paulay, R. Park, and M. J. N. Priestley, "Reinforced concrete beam–column joints under seismic actions," *ACI Structural Journal*, vol. 75, pp. 585–593, 1978.

[10] O. Joh, Y. Goto, and T. Shibata, "Influence of transverse joint and beam reinforcement and relocation of plastic hinge region on beam column joint stiffness deterioration," *ACI Structural Journal*, vol. 123, pp. 187–224, 1991.

[11] S. Fuji and S. Morita, "Comparison between interior and exterior R/C beam–column joint behavior, design of beam–column joints for seismic resistance," *ACI Structural Journal*, vol. 132, pp. 145–166, 1991.

[12] K. Kitayama, S. Otani, and H. Aoyama, "Development of design criteria for RC interior beam–column joints," *ACI Structural Journal*, pp. 97–123, 1991.

[13] B. Li, C. L. Leong, J. W. Baker, H. J. Hwang, H. G. Park, and W. S. Choi, "Comparison between interior and exterior R/C beam–column joint behavior, design of beam–column joints for seismic resistance," *Journal of Structural Engineering*, vol. 132, pp. 145–166, 1991.

[14] S. Pantazopoulou and J. Bonacci, "Consideration of questions about beam–column joints," *ACI Structural Journal*, vol. 89, pp. 27–36, 1992.

[15] J. Bonacci and S. Pantazopoulou, "Parametric investigation of joint mechanics," *ACI Structural Journal*, vol. 90, pp. 61–71, 1993.

[16] H. Noguchi and T. Kashiwazaki, "Experimental studies on shear performances of RC interior column -beam joints with high-strength materials," in *Proceedings of the 10th World Conference on Earthquake Engineering*, pp. 19–24, Madrid, Spain, July 1992.

[17] T. Nagae, W. M. Ghannoum, J. Kwon et al., "Design implications of large-scale shaking table test on four-story reinforced concrete building," *ACI Structural Journal*, vol. 112, no. 2, pp. 135–146, 2015.

[18] H. Shiohara, F. Kobayashi, Y. Sato, and F. Kusuhara, "Earthquake response of multi-story reinforced concrete plane frame structures and seismic design of beam–column joints," *Journal of Structural and Construction Engineering (Transactions of AIJ)*, vol. 82, no. 739, pp. 1437–1447, 2017.

[19] D. M. Cotsovos and M. D. Kotsovos, "Cracking of RC beam/column joints: implications for practical structural analysis and design," *Structural Engineer*, vol. 86, 2008.

[20] D. M. Cotsovos, "Cracking of RC beam/column joints: implications for the analysis of frame-type structures," *Engineering Structures*, vol. 52, pp. 131–139, 2013.

[21] J. Kim and J. M. LaFave, "Key influence parameters for the joint shear behaviour of reinforced concrete (RC) beam–column connections," *Engineering Structures*, vol. 29, no. 10, pp. 2523–2539, 2007.

[22] M. Shin and J. M. Lafave, "Modeling of cyclic joint shear deformation contributions in RC beam–column connections to overall frame behavior," *Structural Engineering & Mechanics*, vol. 18, no. 5, pp. 645–669, 2004.

[23] D. Gombosuren and T. Maki, "Prediction of joint shear deformation index of RC beam–column joints," *Buildings*, vol. 10, pp. 176–234, 2020.

[24] Asce/Sei Committee 41, *Seismic Evaluation and Retrofit of Existing Structures (ASCE/SEI 41-13)*, p. 554, American Society of Civil Engineers, Reston, VA, USA, 2014.

[25] O. C. Celik and B. R. Ellingwood, "Seismic fragilities for nonductile reinforced concrete frames - role of aleatoric and epistemic uncertainties," *Structural Safety*, vol. 32, pp. 1–12, 2010.

[26] A. Ghobarah and A. Biddah, "Dynamic analysis of reinforced concrete frames including joint shear deformation," *Engineering Structures*, vol. 21, no. 11, pp. 971–987, 1999.

[27] P. Zhang, S. Hou, and J. Ou, "A beam–column joint element for analysis of reinforced concrete frame structures," *Engineering Structures*, vol. 118, pp. 125–136, 2016.

[28] O. C. Celik and B. R. Ellingwood, "Seismic risk assessment of gravity load designed reinforced concrete frames subjected to mid-America ground motions," *Journal of Structural Engineering*, vol. 135, no. 4, pp. 414–424, 2009.

[29] B. Bayhan, J. P. Moehle, S. Yavari et al., "Seismic response of a concrete frame with weak beam–column joints," *Earthquake Spectra*, vol. 31, no. 1, pp. 293–315, 2015.

[30] G. M. Calvi, G. Magenes, and S. Pampanin, "Relevance of beam–column joint damage and collapse in RC frame assessment," *Journal of Earthquake Engineering*, vol. 6, no. 1, p. 75, 2002.

[31] B. Bayhan, G. Özdemir, and P. Gülkan, "Impact of joint modeling approach on performance estimates of older-type RC buildings," *Earthquake Spectra*, vol. 33, no. 3, pp. 1101–1123, 2017.

[32] S. Park and K. M. Mosalam, "Simulation of reinforced concrete frames with nonductile beam–column joints," *Earthquake Spectra*, vol. 29, no. 1, pp. 233–257, 2013.

[33] Asce/Sei Committee 7, *Minimum Design Loads and Associated Criteria for Buildings and Other Structures (ASCE/SEI 7-10)*, American American Society of Civil Engineers, Reston, VA, USA, 2010.

[34] Joint Aci-Asce Committee 352, *Recommendations for Design of Beam–Column Connections in Monolithic Reinforced Concrete Structures (ACI-ASCE 352-02)*, American Concrete Institute, Farmington Hills, MI, USA, 2002.

[35] Diana Version 10.3, *TNO Building and Construction Research*, Diana, Delft, The Netherland, 2019.

[36] B. Li and C. L. Leong, "Experimental and numerical investigations of the seismic behavior of high-strength concrete beam–column joints with column axial load," *Journal of Structural Engineering*, vol. 141, no. 9, Article ID 4014220, 2015.

[37] P. Alaee and B. Li, "High-strength concrete interior beam–column joints with high-yield-strength steel reinforcements," *Journal of Structural Engineering*, vol. 143, no. 7, Article ID 4017038, 2017.

[38] B. Li, C. T. N. Tran, and T. C. Pan, "Experimental and numerical investigations on the seismic behavior of lightly reinforced concrete beam–column joints," *Journal of Structural Engineering*, vol. 135, no. 9, pp. 1007–1018, 2009.

[39] J. B. Deaton, *Nonlinear finite element analysis of reinforced concrete exterior beam–column joints with nonseismic detailing*, pp. 1–315, Georgia Institute of Technology, Atlanta, GA, USA, 2013, Ph.D. Thesis.

[40] M. A. N. Hendriks, A. de Boer, and B. Belletti, "Guidelines for nonlinear finite element analysis of concrete structures," Rijkswaterstaat Cent Infrastructure, The Netherlands, RTD, 10162012 2020, 2020.

[41] D. A. Hordijk, *Local approach to fatigure of concrete*, Ph.D. Thesis, Delft University of Technology, Delft , The Netherland, 1991.

[42] Fib, *FIB Model Code for Concrete Structures 2010*, International Federation for Structural Concrete, Lausanne, Switzerland, 2013.

[43] H. Nakamura and T. Higai, "Compressive fracture energy and fracture zone length of concrete, Modelling of inelastic behavior of R.C. structures under seismic loads edited by Shing P, Tanabe T," *ASCE*, vol. 10, pp. 471–487, 1999.

[44] F. J. Vecchio and M. P. Collins, "Compression response of cracked reinforced concrete," *Journal of Structural Engineering*, vol. 119, no. 12, pp. 3590–3610, 1993.

[45] R. G. Selby, F. J. Vecchio, and M. P. Collins, "Analysis of reinforced concrete members subject to shear and axial compression," *ACI Structural Journal*, vol. 93, pp. 306–315, 1996.

[46] H. Sucuoğlu and M. S. Günay, "Generalized force vectors for multi-mode pushover analysis," *Earthquake Engineering & Structural Dynamics*, vol. 40, no. 1, pp. 55–74, 2011.

[47] M. Kreslin and P. Fajfar, "The extended N2 method taking into account higher mode effects in elevation," *Earthquake Engineering & Structural Dynamics*, vol. 40, no. 14, pp. 1571–1589, 2011.

[48] A. Habibi, H. Saffari, and M. Izadpanah, "Optimal lateral load pattern for pushover analysis of building structures," *Steel and Composite Structures*, vol. 32, 2019.

[49] Y. Liu and J. S. Kuang, "Spectrum-based pushover analysis for estimating seismic demand of tall buildings," *Bulletin of Earthquake Engineering*, vol. 15, no. 10, pp. 4193–4214, 2017.

[50] J. Z. Zhang, J. Jiang, and G. Q. Li, "An improved consecutive modal pushover procedure for estimating seismic demands of multi-storey framed buildings," *The Structural Design of Tall and Special Buildings*, vol. 26, no. 4, p. e1336, 2017.

[51] A. K. Chopra and R. K. Goel, "A modal pushover analysis procedure to estimate seismic demands for unsymmetric-plan buildings," *Earthquake Engineering & Structural Dynamics*, vol. 33, no. 8, pp. 903–927, 2004.

[52] T. D. Ancheta, R. B. Darragh, J. P. Stewart, W. Silva, B. Chiou, and K. Wooddell, "PEER NGA-west2 database," Pacific Earthquake Engineering Research center, Berkeley, CA, USA, PEER 2013/03, 2013.

[53] Venture N C J Nist, *GCR 11-917-15-selecting and Scaling Earthquake Ground Motions for Performing Response-History Analyses*, US National Institute for Standards and Technology, Gaithersburg, MD, USA, 2011.

[54] W. K. Tso, T. J. Zhu, and A. C. Heidebrecht, "Engineering implication of ground motion A/V ratio," *Soil Dynamics and Earthquake Engineering*, vol. 11, no. 3, pp. 133–144, 1992.